# A novel mechanism of "metal gel-shift" by histidine-rich $Ni^{2+}$-binding Hpn protein from *Helicobacter pylori* strain SS1

**Short Title:**

Physicochemical aspects of a histidine-rich protein, Hpn

Rahul Mahadev Shelake[1], Yuki Ito[1], Junya Masumoto[1], Eugene Hayato Morita[2,3], Hidenori Hayashi[1]*

[1]Proteo-Science Center, Ehime University, Matsuyama, Japan

[2]Laboratory of Molecular Cell Physiology, Faculty of Agriculture, Ehime University, Matsuyama, Japan

[3]Department of Chemistry, Faculty of Science, Josai University, Saitama, Japan

***Corresponding author:**

E-mail: hayashi.hidenori.mj@ehime-u.ac.jp (HH)

# Abstract

Sodium dodecyl sulphate-polyacrylamide gel electrophoresis (SDS-PAGE) is a universally used method for determining approximate molecular weight (MW) in protein research. Migration of protein that does not correlate with formula MW, termed “gel shifting” appears to be common for histidine-rich proteins but not yet studied in detail. We investigated “gel shifting” in $Ni^{2+}$-binding histidine-rich Hpn protein cloned from *Helicobacter pylori* strain SS1. Our data demonstrate two important factors determining “gel shifting” of Hpn, polyacrylamide-gel concentration and metal binding. Higher polyacrylamide-gel concentrations resulted in faster Hpn migration. Irrespective of polyacrylamide-gel concentration, preserved Hpn-$Ni^{2+}$ complex migrated faster (3-4 kDa) than apo-Hpn, phenomenon termed “metal gel-shift” demonstrating an intimate link between $Ni^{2+}$ binding and “gel shifting”. To examine this discrepancy, eluted samples from corresponding spots on SDS-gel were analyzed by matrix-assisted laser desorption/ionization-time-of-flight mass spectrometry (MALDI-TOF-MS). The MW of all samples was the same (6945.66±0.34 Da) and identical to formula MW with or without added mass of $Ni^{2+}$. MALDI-TOF-MS of $Ni^{2+}$-treated Hpn revealed that monomer bound up to six $Ni^{2+}$ ions non-cooperatively, and equilibrium between protein-metal species was reliant on $Ni^{2+}$ availability. This corroborates with gradually increased heterogeneity of apo-Hpn band followed by compact "metal-gel shift" band on SDS-PAGE. In view of presented data metal-binding and “metal-gel shift” models are discussed.



# Key words

Histidine-rich protein; Hpn; nickel; anomalous SDS-PAGE migration; gel shifting on SDS-PAGE; MALDI-TOF-MS; protein-metal ion complex.

# Introduction

Cysteine-rich (-SH group) metal-binding proteins, for example metallothioneins, are known to bind and sequester multiple metal ions in prokaryotes and eukaryotes [1], but understanding of histidine-rich (imidazole group) metal-binding proteins is still limited. Proteins with histidine-rich repeats are universally present in the proteomes of both prokaryotes and eukaryotes, including human, and form unique single-residue-repeat motifs [1,2]. *Helicobacter pylori*, a human pathogen responsible for severe gastric diseases including intestinal ulcers and adenocarcinoma, requires two key Ni-containing enzymes (urease and hydrogenase) for survival in acidic gastrointestinal conditions [3]. Thus, *H. pylori* produce unique $Ni^{2+}$-binding histidine-rich proteins required in the maturation of urease and hydrogenase.

One of the first candidates involved in $Ni^{2+}$ homeostasis in *H. pylori* was isolated and named Hpn (*Helicobacter pylori* protein binding to nickel) [4]. Hpn contains 28 histidine residues (46.7%) with two stretches of repeated histidines at positions 11-17 and 28-33 (**Fig 1A**). It also contains two short repeating motifs (EEGCC) in the internal part positioned at 38-42 and 51-55. The relative affinity of Hpn towards divalent metal ions was found to be different under *in vivo* and *in vitro* conditions indicating the complex nature of the protein [4–7]. Initial Hpn mutation studies in *H. pylori* showed that the mutant strain was more sensitive to $Ni^{2+}$ than a wild-type strain [4,8,9]. Inductively coupled plasma-mass spectrometry and equilibrium dialysis studies revealed that average five $Ni^{2+}$ ions (5.1±0.2) bind to Hpn in a pH-dependant manner and forms a range of multimeric complexes (>500, 136, 55, 34, 26, 20, 14 and 7 kDa) in solution that exists in equilibrium depending on buffer content [5,6]. The pH titration and competition experiments using EDTA confirmed that the metal-binding to Hpn is a reversible process [5–7]. Even though some amino-acid residues vital for metal-binding were identified [10–12], distribution of metal-binding sites and equilibrium between

protein-metal species in Hpn is not yet known. Hpn may act in $Ni^{2+}$ storage as a 'reservoir' or in channelizing $Ni^{2+}$ to other proteins [5,6,13]. Purified Hpn can form amyloid-like fibers *in vitro* [14] but such fibers yet to be established *in vivo* in *H. pylori*. A recent study described Hpn interaction with Hpn-2 (also known as Hpn-like or Hpn-l, another atypical histidine-rich protein with MW 8.07 kDa [15]) mediate urease activity [13]. Thus, considering several complex chemical interactions, Hpn can be employed as an ideal protein to investigate metallochemistry and physicochemical aspects of histidine-rich metal-binding proteins.

Even though sodium dodecyl sulfate-polyacrylamide gel electrophoresis (SDS-PAGE) is the most commonly used method for the determination of approximate MW of proteins; unusual electrophoretic behavior in SDS-PAGE has been reported for Hpn, making its identification problematic [5]. This phenomenon of unpredictable migration rate on SDS-PAGE against actual formula MW of protein is termed "gel shift" (not to be confused with the electrophoretic mobility shift assay for protein-DNA interactions). The "gel shifting" has also been reported for several other histidine-rich proteins including Hpn [5], UreE [16], HypB [17–19], SlyD [20,21], Hpn-like [9], and CooC [22] **(Table 1)** as well as different helical membrane proteins [23–25] including some isobaric peptides (peptides with the same MW) from various organisms [26]. HspA from *Helicobacter*, which has a unique C-terminus containing a histidine-rich region, also exhibited a higher MW of 15.5 kDa than the expected 13 kDa [27] indicating that the "gel shift" behavior might be attributable to histidine-rich region. However, the molecular mechanism is yet to be clarified. Six possible mechanisms responsible for "gel shifting" of a protein have been hypothesized in previous reports: (a) divergent higher order (secondary or tertiary) structure; (b) difference in Stokes-Einstein (hydrodynamic) radius of the protein-surfactant complex; (c) variation in the intrinsic net charge of the protein; (d) number of bound SDS molecules; (e) post-translational modifications; or (f) binding of cofactors such as metal ions to the protein [23–25,28–30].

Nevertheless, polyacrylamide-gel concentration can dictate magnitude and direction of some proteins in SDS-gel [31].

**Table 1. List of histidine-rich $Ni^{2+}$-binding proteins showing gel shifting anomaly.**

| Protein | Organism | Function | Histidine content | Ni ions per monomer | Formula MW (kDa) | Apparent MW (kDa) | Reference |
|---|---|---|---|---|---|---|---|
| SlyD | *Escherichia coli* | Ni carrier | 10.2% | 3 | 20.8 | 25 | [20,21] |
| CooC | *Rhodospirillum rubrum* | Nickel accessory protein for maturation of CODH | 3% | 1 | 27.8 | 61, 29 | [22] |
| HypB | *Rhizobium leguminosarum* | GTP-dependent Ni insertase | 9.0% | 4 | 32.5 | 39 | [18,19] |
| HypB | *Archeoglobus fulgidus* | GTP-dependent Ni insertase | 2.7% | 0.5 | 24.7 | 41 (dimer) | [17] |
| UreE | *Klebsiella aerogenes* | Accessory protein in urease maturation | 9.5% | 3 | 17.5 | 35 (dimer) | [16] |
| Hpn like | *Helicobacter pylori* | Ni storage | 25% | 2 | 9 | 47, 18 | [9] |
| Hpn | *Helicobacter pylori* | Ni storage | 46.7% | 5-6 | 7 | >670, 500, 230, 136, 20, 14, 7 | Present study and [5] |

Recently, attempts have been made to investigate these molecular mechanisms using segments of various membrane proteins, and the findings indicated that there might be no single universal mechanism that accounts for the anomalous migration of all proteins. In fact, each protein or class of proteins may have unique chemistry responsible for “gel shifting” behavior. It is an interesting question that whether “gel shifting” in Hpn is linked to the displacement of protein-protein, protein-metal, and/or protein-SDS interactions, but these need further investigation.

We cloned the *hpn* gene from the Sydney Strain 1 (SS1) of *H. pylori*, a standardized mouse model [32]. Our preliminary data demonstrated the altered migratory position for Hpn on SDS-PAGE when Hpn was expressed in $Ni^{2+}$-supplied medium suggesting role of $Ni^{2+}$ in altered migration. We find that the migration rate of $Ni^{2+}$-treated Hpn on SDS-PAGE was

112 altered because of preserved protein-metal complexes. Preservation of intact protein-metal
113 bond in non-denaturing conditions is commonly reported [33,34]. SDS-PAGE is primarily
114 designed to separate denatured proteins by disrupting non-covalent complexes. However, in
115 SDS-treated samples, protein under study and proteins used as MW standards attain
116 equivalent shape not by an absolute unfolding but indeed it is achieved by the SDS
117 aggregation at hydrophobic sites [23]. Thus, protein denaturation occurs in ‘‘reconstructive’’
118 manner and it forms a mixture of SDS micelle wrapped around α-helices separated by linkers
119 (necklace and bead model) or hydrophobic regions of protein wrapped around SDS micelles
120 (decorated micelle model), both reviewed in [35]. Thus, some SDS-resistant protein-protein
121 interactions (**supporting information, S1 Table in S1 file**) and protein-metal complexes
122 (**supporting information, S2 Table in S1 file**) can also preserve in electrophoretic separation
123 upon SDS-PAGE provided interaction is stronger [34]. Also, many studies reported that the
124 “reconstructive” denaturation can retain some protein-metal complexes on SDS-PAGE but
125 altered migration is not generally observed except for some $Ca^{2+}$-binding proteins such as
126 calmodulin isoforms [36] and $Ca^{2+}$-dependent protein kinases (CDPKs) [37–40]. Overall, the
127 above observations suggest that there may be an apparent link between metal-binding to Hpn
128 and “gel shifting” pattern. Thus, the anomalous migration of Hpn should be explored in
129 several conditions pertaining to metal binding and its effect on migration rate in SDS-PAGE.
130 Also, MW of intact Hpn alongside protein-metal interaction studies by MS could facilitate
131 better understanding of Hpn metallochemistry in detail.

132 In the present study, an attempt was made to investigate various physicochemical
133 properties of Hpn and not the *in vivo* function of Hpn in *H. pylori* itself. This work was
134 focused on heterologous expression of Hpn in *E. coli*, average molecular mass of purified
135 Hpn, “gel shifting” anomaly with or without $Ni^{2+}$ in different polyacrylamide-gel
136 concentrations and application of MALDI-TOF-MS for studying non-covalent Hpn-$Ni^{2+}$

complexes. To establish a reliable technique to determine MW associated with "gel shifting" anomaly without ambiguity, MW of intact recombinant Hpn was determined by MALDI-TOF-MS using internal protein standards and found to be essentially identical (6945.66±0.34) to the formula MW. $Ni^{2+}$-treated Hpn migrated more rapidly than untreated Hpn showing differences of 3-4 kDa. This significant metal-triggered shift in electrophoretic gel mobility of Hpn is reported for the first time to the best of our knowledge and termed as a "metal gel-shift". Migration speed of Hpn in both the forms was altered depending on polyacrylamide-gel concentrations. The method for sample and matrix preparation standardized in this study preserved appropriate intermolecular interactions and hence boosts the usefulness of MALDI for the study of non-covalent protein-metal ion complexes.

# Materials and Methods

## *H. pylori* strain and growth conditions

All the chemicals and reagents used were of analytical grade or higher. The mouse-adapted strain of *Helicobacter pylori* Sydney strain (*H. pylori* SS1) was used in this study [32]. *H. pylori* SS1 was grown on Tripticase Soy agar with 5% sheep blood (TSA II) (Becton Dickinson, Franklin Lakes, NJ) for three days at 35ºC in 12% carbon dioxide condition. A single colony was isolated and sub-cultured on TSA II agar at 35ºC in 12% carbon dioxide condition.

## Purification of DNA from *H. pylori* strain SS1

The genomic DNA from strain SS1 was extracted based on phenol-chloroform method as described previously [32] with minor modifications. Briefly, bacteria were harvested from TSA II agar and suspended in 3 ml of Tris-buffered saline (TBS). After washing with TBS once by centrifugation at 3,800 g for 5 min at 4ºC, 5 x $10^8$ colony forming unit (CFU) of bacteria were re-suspended in 500 µl of lysis buffer (50 mM Tris-HCl, pH 8.0; 100 mM EDTA, pH 8.0; 1 % SDS, 100 mM NaCl) containing 0.2 mg/ml proteinase K (Amaresco, Solon, OH) and incubated at 37ºC for 12 h. Subsequently, UltraPure™ buffer-saturated phenol (Invitrogen, Carlsbad, CA) was added, and the mixture was gently rotated for 15 min. After centrifugation, the aqueous phase was transferred to a tube containing chloroform/isoamyl alcohol (24:1, Sigma-Aldrich, St. Louis, MO) and agitated gently for 10 min. The aqueous phase was collected to a new tube by centrifugation. The DNA was precipitated by addition of isopropyl alcohol and 0.3 M sodium acetate, and then the DNA pellet was rinsed with 70% ethanol. After centrifugation, pellet was air-dried and dissolved in Tris-EDTA buffer (pH 8.0).

## Cloning and nucleotide sequencing

First, the Hpn encoding region of 1.17 kb was amplified instead of the *hpn* gene only to avoid undesired mutations in the nucleotide sequence of *hpn* (primers 5'-AGTCCATATGCCTTACACGCCGTAGATGACAAAACGCGC-3' and 5'-GACTGGATCCGGCTCGCTCTCATCTATAGCGTGGCTAAG-3'). The DNA fragment was cloned into a pBluescript II KS (+) vector (Takara, Japan), and nucleotide sequencing was performed using a BigDye Terminator v3.1 Cycle Sequencing Kit and an ABI PRISM 310 Genetic Analyzer (Applied Biosystems). The *hpn* gene was amplified using the cloned 1.17 kb region as the PCR template (primers 5'-GACTCATATGGCACACCATGAAGAACAACAC-3' and 5'-GACTGGATCCTTATTACTCGTGATGCCCGTGGC-3') and then cloned into pBluscript (Takara, Japan) and pET21b (Novagen, Darmstadt, Germany) vectors. *E. coli* JM 109 and BL21 (DE3) cells purchased from Takara (Japan) were used for the propagation and protein expression with a constitutive (RuBisCo promoter from *Synechococcus* sp. PCC7002) [41]; and isopropyl β-D-1-thiogalactopyranoside (IPTG)-inducible T7 promoter, respectively.

## Expression and purification of recombinant Hpn

Recombinant Hpn was purified from harvested cells of 200 ml culture. Harvested cells were suspended in lysis buffer (50 mM Tris-HCl, pH 7.5, and 500 mM NaCl) and purification was done as described previously for His-tagged proteins with some modifications [42]. After sonication (TOMY Ultrasonic Disruptor, duty: 50, output: 4, time: 4 min x 6), supernatant fractions were filtered using Millex®GV filter units of 0.22-µm-pore-size and applied onto a 1-ml HiTrap chelating column (GE Healthcare) that had been equilibrated with start buffer containing 20 mM imidazole, 50 mM Tris-HCl, and 500 mM NaCl. The column was washed with buffer (50 mM Tris, pH 7.5, 50 mM NaCl, and 40 mM imidazole), and then Hpn was eluted using start buffer with 400 mM instead of 20 mM imidazole. Eluted fractions were analyzed for purity using SDS-PAGE (15%), and the purest

fractions were applied onto a 5-ml HiTrap desalting column (GE Healthcare) that had been equilibrated with desalting buffer (20 mM Hepes-KOH, pH 7.4, 100 mM NaCl, and 20% glycerol), and purified Hpn was stored at −80ºC until use. The concentration and quality of purified Hpn was measured using bovine serum albumin (BSA) as the standard in a BCA assay (Bio-Rad) in accordance with the manufacturer's instructions and SDS-PAGE (polyacrylamide 15%), respectively.

## SDS-PAGE and non-denaturing native-PAGE (native-PAGE)

All purified protein fractions were analyzed by SDS-PAGE in accordance with instructions mentioned previously [43]. A vertical electrophoresis system of mini-slab size from Atto Co. (Japan) was used for the separation of protein samples with appropriate concentrations of polyacrylamide. A LMW-SDS Marker Kit (GE Healthcare) and marker proteins kit from Nacalai Tesque, Inc. (Japan) were used as protein standards in SDS-PAGE. All protein samples were prepared in Laemmli buffer (50 mM Tris-HCl pH 6.8, 10% glycerol, 2% SDS, 7% β-mercaptoethanol and 0.001% bromophenol blue) and then stored at −20ºC before use. The electrophoresis was done till bromophenol blue dye reached to the bottom in all gels of different concentrations (under similar experimental conditions). This optimized method was referred from previous work [31] showing separation of 11 trans-membrane mimetic peptides, translating into MWs of 3.5-41 kDa on 11-18% of polyacrylamide-gel. Resolved proteins were stained with Coomassie Brilliant Blue (CBB) R-250 solution containing 10% acetic acid with 25% methanol.

Fractions of purified Hpn were used for blue native PAGE analysis without boiling or reduction in sample buffer (50 mM Tris with pH 6.8 containing 0.01% bromophenol blue and 10% glycerol). The running buffer was prepared without detergent and consisted of 25 mM Tris, 192 mM glycine, pH 8.0. Stacking gel (4%) and separation gel (10%) were prepared adding suitable buffers, glycerol, ammonium persulfate (APS), and TEMED. Electrophoresis

was performed at a constant current of 15 mA and voltage of 160 V and further CBB stained.

## Western blotting analysis

The Hpn protein (25 µM) treated with indicated mol equivalent of EDTA or $Ni^{2+}$ resolved on SDS-PAGE (20%) and then electrophoretically blotted onto polyvinylidene fluoride (PVDF) membrane (Amersham Hybond-P, GE Healthcare, code: RPN303F) in transfer buffer containing no methanol. Blotting was performed at 0.8 mA current for every $cm^2$ area of gel. Proteins were blocked on PVDF membranes in a solution of 5% skim milk for 1 h after washing in PBS-T buffer (phosphate-buffered saline buffer with 0.05% Tween-20, pH 8). The PVDF membrane was further incubated with C-terminal specific-anti 6×histidine monoclonal antibody (9F2) (Wako Japan, product code: 010-21861 diluted to 1:5000 in PBS-T) for 1 h. After three washes of 15:5:5 min in PBS-T, PVDF membrane was then incubated with horseradish peroxidase-conjugated anti-mouse IgG (GE Healthcare, product code: NA931VS, diluted to 1:5000 in PBS-T) for 1 h. The membrane was further washed again with PBS-T as mentioned earlier and Amersham ECL non-radioactive western blotting detection reagents (GE Healthcare) were used for visualizing protein bands in accordance with the manufacturer's instructions.

## Enzyme-linked immunosorbent assay (ELISA) analysis

Green fluorescent protein with artificial His.tag (*gfp-His$_6$*) and GFP fused with Hpn (*gfp-Hpn*) were cloned in pET21b. IPTG-induced over-expression of both the proteins was done with or without $Ni^{2+}$ added in the culture (**Supporting information, S1 Fig in S1 file**). Pellets of 60 µl bacterial cultures were dissolved in 60 µl sample buffer and incubated for 3 min at 100ºC. Final volume of 15 µl loaded in each lane for SDS-PAGE. ELISA experiment was performed using previously described protocol with some modifications [44]. Different buffers were prepared before starting ELISA experiment (components of buffers summarized in Table 2).

**Table 2. Components of different buffers used in ELISA.**

| Buffer type | Components |
|---|---|
| Coating buffer | Phosphate buffer saline, [1.16 g $Na_2HPO_4$, 0.1g KCl, 0.1 g $K_3PO_4$, 4.0 g NaCl (500 ml distilled water) pH 7.4] |
| Dilution buffer | 0.1% BSA with 0.05% Tween-20 in PBS |
| Blocking buffer | 1% BSA with 0.05% Tween-20 in PBS |
| Washing buffer | 0.05% Tween-20 in PBS |
| Stop buffer | 5N Sodium Hydroxide in distilled water |

Flat-bottom 96-well ELISA plates (untreated 96-well microplates from Falcon) were used for coating. Concentration of each protein (Hpn, GFP-Hpn and GFP-$His_6$) was adjusted to 1 µg by dilution with coating buffer to the final volume of 50 µl. Plates were incubated at 4ºC for overnight. Next day, solution was thrown away and 200 µl blocking buffer into each well was added. Then, plate was incubated at 37ºC for 1hr. After incubation, solution was discarded and plate was washed three times by washing buffer. His.Tag® antibody was diluted to standardized concentration (1:500) with dilution buffer [C-terminal specific-anti 6xhistidine monoclonal antibody (9F2) (Wako Japan, product code: 010-21861)] and plate incubated at 37ºC for 1hr after adding 100 µl in each well. After three washes with wash buffer, plate was incubated with horseradish peroxidase-conjugated anti-mouse IgG (GE Healthcare, product code: NA931VS, diluted to 1:1000 in wash buffer) for 1 hr at 37ºC. After similar washing, the substrate ABTS [2,2'-Azinobis(3-ethylbenzothiazoline-6-sulfonic Acid Ammonium Salt) from Wako Japan] dissolved in 0.1 M citrate buffer and hydrogen peroxide (0.03%) was added. Then the plate was incubated for 20 minutes at room temperature. Reactions were stopped by adding stop buffer (100 µl) in each well. The absorbance at 415 nm was measured using a Spectramax M3 microplate reader (Molecular Devices Co., Sunnyvale, CA). Values obtained (absorbance at 415 nm) for $Ni^{2+}$-treated samples (from

279 average of at least three replications) were normalized against untreated samples and plotted
280 in graph.

## 281 Hpn interaction with $Ni^{2+}$ ions

282 For SDS-PAGE and blue native-PAGE analysis, apo-Hpn (25 µM) was prepared as
283 mentioned above and then treated with the indicated amount of $Ni^{2+}$ by adding $NiSO_4$
284 solution or EDTA (with mol equivalent ratio of 1:6) and incubated for a minimum of 1 h at
285 room temperature. Suitable PAGE buffer was added to the above mixture for loading either
286 on SDS-PAGE (Laemmli buffer) or blue native PAGE (sample buffer used, 50 mM Tris, pH
287 6.8 with 10% glycerol and 0.01% bromophenol blue). Equal volume of 2X loading buffer
288 was added to protein samples and then applied to native-PAGE directly. For SDS-PAGE,
289 further processing (heat denaturation) done otherwise mentioned in respective figures. $Ni^{2+}$
290 binding to Hpn protein was investigated using MALDI-TOF-MS by mixing $Ni^{2+}$ or EDTA-
291 treated Hpn with equal amount of matrix solution.

292 The gel slices of EDTA or $Ni^{2+}$-treated protein bands resolved on SDS-gel were
293 digested in nitric acid (Nacalai Tesque, Japan) and heated at 80ºC for 10 min, once cooled
294 nitric acid finally diluted to 2%. The $Ni^{2+}$ content was analyzed by ICP-optical emission
295 spectrometry (ICP-OES) (Optima 8300 ICP-OES Spectrometer, PerkinElmer Inc, USA). The
296 standard curve was plotted using a minimum of five standards (ranging from 50 to 1000 ppm)
297 with a blank of 2% nitric acid.

## 298 MALDI-TOF-MS

299 Protein bands resolved on SDS-PAGE were eluted using the protocol described
300 previously [45] with or without CBB staining and then aliquots were used in mass
301 spectrometry. Purified Hpn and elution fractions were directly mixed with an equal volume of
302 matrix solution prepared with different recipes. Acidic and non-acidic matrices were
303 investigated for detecting intact protein-metal ion complexes. Acidic matrix was prepared by

mixing 100% acetonitrile (ACN), 0.1% trifluoroacetic acid (TFA), and distilled water (v:v, 50:10:40). Another mild acidic matrix was prepared with the recipe except for more diluted 0.01% TFA. Two different non-acidic matrices were analyzed: 1) sinapinic acid in 100% ACN and distilled water (v:v, 1:1) without TFA [46]; and 2) 4-hydroxy-α-cyanocinnamic acid powder in a saturated solution of ethanol and 1 M ammonium acetate (v:v, 1:1) [47]. MALDI-TOF-MS analysis was done with a Voyager-DE PRO MALDI-TOF-MS (Applied Biosystems). The instrument was calibrated externally with a Sigma Protein MALDI-MS calibration kit. The positive linear mode was set in the instrument to acquire mass spectra using a nitrogen laser (337 nm). An average of a minimum of 150 laser shots was used to accumulate a single spectrum with an accelerating voltage of 25,000 V and extraction delay time of 400 ns. Internal calibration with protein standards (insulin and apomyoglobin), smoothing and baseline correction of the mass spectra was performed and analyzed by using Data Explorer software (Applied Biosystems, MA).

## Effect of $Ni^{2+}$ on growth of *E. coli* expressing the *hpn* gene

*E. coli* cultures, both with pBluscript only and pBluscript-*hpn* plasmid inoculated from individual colonies were grown for overnight in Luria-Bertani (LB) medium containing 100 μg/ml ampicillin at 37ºC. Optical density (OD) of the grown cultures was measured at 600 nm and normalized to 1, of which 100 μl was inoculated to 5 ml of fresh LB medium (1:50 dilution) containing 100 μg/ml ampicillin, and $NiSO_4$ was added where applicable (0, 500, 1000, 1200 μM). Cultures were grown for 4 h at 165 rpm at 37ºC, OD values were measured using U-1800 spectrophotometer (Hitachi, Japan) at 600 nm. Obtained values were normalized against control (culture grown without $Ni^{2+}$ stress) and data from three different replicates was summarized and used to plot the growth curve.

M9 medium is a minimal defined culture medium prepared as described previously [48]. Overnight grown cultures (as above, 100 μl) were inoculated into 5 ml of fresh M9

329 medium containing 0, 50, and 100 μM $NiSO_4$ and 100 μg/ml ampicillin. These cultures were
330 incubated for 24 h at 165 rpm at 37ºC in a shaker and the growth curve was plotted (as
331 described above).

## 332 $Ni^{2+}$ accumulation in *E. coli* expressing the *hpn* gene

333 Single colonies of transformed *E. coli* JM109 were inoculated into 2 ml of fresh
334 medium (LB or M9) supplemented with appropriate concentrations of $Ni^{2+}$. Overnight grown
335 cultures (after normalizing OD to 1) were inoculated into 5 ml of fresh medium and grown
336 for 24 h at 37ºC with and without $Ni^{2+}$. Sampling (2 ml culture) was done at 24 h (LB and
337 M9), respectively. Cells were centrifuged at 15000 rpm for 1 min and bacterial pellet was
338 washed with GET buffer (50 mM glucose, 25 mM Tris-HCl, 10 mM EDTA) followed by
339 drying at 80ºC for a minimum of 3 h. The dried pellet was digested in nitric acid (Nacalai
340 Tesque, Japan) and heated at 80ºC for 10 min, once cooled nitric acid finally diluted to 2%.
341 The $Ni^{2+}$ content incorporated inside the cell and total uptake were analyzed by ICP-OES.
342
343
344
345
346
347
348
349
350
351
352
353

# Results

## Overexpression and purification of Hpn

Four changes were observed at the nucleotide level in the *hpn* ORF of strain SS1 compared with strain 26695, but it had no change at the amino-acid level (**Supporting information, S2 Fig in S1 file**). Hpn expression in *E. coli* culture was standardized in LB medium. The molecular mass of Hpn expressed with and without $Ni^{2+}$ was investigated by SDS-PAGE with a crude cell extract and found to be different (**Fig 1B**). The SDS-PAGE pattern of imidazole-eluted Hpn showed three major protein bands of approximately 14 kDa, 18 kDa, and 70 kDa on 15% polyacrylamide-gel (**Fig 1C**). The SDS-resistant oligomeric complex (~70 kDa) was highly stable and unaffected by reducing agents such as β-mercaptoethanol or boiling (100ºC for 3 min). After desalting, this ~70 kDa band was observed but at very low concentration, thereby suggesting the role of imidazole in inter-conversion of Hpn multimeric forms (**Fig 1D**). The other two protein bands of ~14 kDa and ~18 kDa were observed corresponding to the pattern of the crude extract with and without $Ni^{2+}$ respectively. This indicates that a trace of $Ni^{2+}$ was present in purified Hpn incorporated during the purification process. Thus, the purified Hpn was used after removing trace amounts of $Ni^{2+}$ by treating with EDTA during buffer exchange with desalting columns (**Fig 1E**).

**Fig 1. Amino acid sequence, overexpression and purification of recombinant Hpn.**
Lane M, LMW protein marker standards (GE Healthcare); black arrows depicting apo-Hpn and white arrows showing probable $Ni^{2+}$-bound Hpn protein in all panels.
A. Amino acid sequence of Hpn. Histidine residues are highlighted in bold. Stretches of six and seven histidines are highlighted in green and pentapetide repeats (EEGCC) are underlined.
B. SDS-PAGE of Hpn expression with or without $Ni^{2+}$ added in the culture (polyacrylamide-

gel 20%). Pellets of 60 µl bacterial cultures were dissolved in 60 µl of 1X Laemmli buffer and boiled for 3 min at 100ºC. Final volume of 15 µl loaded in each lane.
C, D and E. Elution profile of purified Hpn checked by loading protein fractions on SDS-PAGE (polyacrylamide-gel 15%). Lanes 1 to 10, fractions of purified protein eluted with 400 mM imidazole (C). Elution profiles of desalted fractions of Hpn without EDTA treatment (D) and with EDTA-treatment (E) were analyzed. Equal volume of 2X Laemmli buffer was added to each eluted fraction and then boiled for 3 min at 100ºC. Total 10 µl applied in each lane in C, D and E.

It has been shown that Hpn forms a range of multimeric complexes depending on buffer composition and treatment of DTT, imidazole and $Ni^{2+}$ estimated by gel-filtration chromatography [5]. Consistent with earlier report, Hpn protein (25 µM) treated with either EDTA or $Ni^{2+}$ (mol equivalent ratio of 1:6 independently) migrated as a range of multimeric species on 10% native-PAGE gel (**Supporting information, S3Fig in S1 file**).

## Confirmation of recombinant Hpn by Western blotting

The post-translational removal of N-terminal methionine (149.21 Da) in wild-type (in *Helicobacter pylori*) and recombinant Hpn (in *E. coli*) is reported [4,5]. Therefore, the monoisotopic and average molecular mass (abbreviated as $M_{MONO}$ and $M_{av}$) of Hpn without N-terminal methionine were estimated using PAWS software (http://www.proteometrics.com) as 6941.288 Da and 6946.01 Da, respectively. Hpn appeared to migrate faster in the sample from cells cultured with $Ni^{2+}$ compared to that without $Ni^{2+}$ on 15% (**Fig 1C-E**) or 20% SDS-PAGE (**Fig 1B**), but neither of the conditions showed the migratory position for an expected MW i.e. ~7 kDa.

To facilitate the identification of Hpn protein (untagged) precisely, western blotting was performed using a His.Tag® monoclonal antibody assuming that the His.Tag® antibody would bind to Hpn at the seven and six residue histidine repeats [5]. Recombinant Hpn (untagged) confirmed a thin band in western blot (**Fig 2A**, left panel) corresponding to the

migration position of apo-Hpn but $Ni^{2+}$-treated Hpn was barely visible. CBB staining of same PVDF membrane showed both the protein bands but small amount of $Ni^{2+}$-treated Hpn remain bound to membrane (**Fig 2A**, right panel). Possible explanation is that untagged Hpn, specifically metalated form may have weaker binding affinity to membrane probably due to its atypical chemical nature.

**Fig 2. Western blot and ELISA analysis of Hpn, GFP-$His_6$ and GFP-Hpn.**

A. Western blot of Hpn was done using His.Tag® monoclonal antibody. In left panel, X-ray sheet showing ECL detection result of recombinant Hpn (with and without $Ni^{2+}$) and right panel showing same CBB-stained-PVDF membrane used for ECL detection.

B. Western blot of untagged Hpn, GFP-Hpn and GFP-$His_6$ on PVDF membrane either treated with or without $Ni^{2+}$ solution (1mM of $NiSO_4$).

C. ELISA of denatured untagged Hpn, GFP-Hpn and GFP-$His_6$ Equal amount of protein (1 µg) was coated on ELISA plate. His.Tag® antibody was diluted to 1:500 for detection. Values obtained (absorbance at 415 nm) for $Ni^{2+}$-treated samples (from average of at least three replications) were normalized against untreated samples and plotted in graph. Paired t-test was performed to compare the metal ion effect, ** indicate $p<0.01$.

## Metal-binding to Hpn changes Hpn-antibody interaction

Interaction of His.Tag® antibody with Hpn may not necessarily show similar results for other protein having artificial His.Tag or Hpn conjugated with another protein owing to differential co-ordination geometry of metal-binding and its chemical surrounding. We investigated this possibility using GFP- $His_6$ and GFP-Hpn (**Fig 2B**). GFP does not interact with His.Tag® antibody by its own. GFP is comparatively large protein (26.7 kDa) but still positional shift was observed in case of GFP-Hpn expressed in LB medium supplied with $Ni^{2+}$. Western blot data of GFP-$His_6$ and GFP-Hpn showed almost equal intensity signals in both the cases i.e. with or without $Ni^{2+}$.

Recognition site for His.Tag® antibody is $His_6$ peptide attached at C-terminal of a

recombinant protein and it is a linear epitope. Hence, conformational change upon $Ni^{2+}$-binding to Hpn may lead to altered binding of His.Tag® antibody. This was further examined by ELISA using His.Tag® antibody (**Fig 2C**). The SDS-treated and non-treated Hpn protein shown similar results which is compatible with previous observations for several other proteins [49,50]. The relative detection sensitivity of $Ni^{2+}$-treated protein with His.Tag® antibody in ELISA give order of untagged Hpn < GFP-Hpn < GFP-$His_6$. Hence, the variability that we observed in detection of apo- and metalated-Hpn on western blots may have resulted not only from membrane-binding efficiency but also from differential exposure of His-rich region upon metal-binding.

These data signify that the metal-binding to Hpn causes altered binding of His.Tag® antibody, possibly due to change in protein confirmation.

## Determination of MW by MALDI-TOF-MS

To quantify the reliable molecular mass of untagged Hpn, MALDI-TOF-MS was used for purified apo-Hpn with an acidic matrix in linear positive mode. As shown in **Fig 3A**, integral signals of four heteromeric species of Hpn ($M^+$, $2M^+$, $3M^+$, and $4M^+$) were observed with a major peak of singly charged Hpn[$M^+$]. Although a tendency of apo-Hpn to form multimeric complexes in native and reduced states was confirmed by native-PAGE and SDS-PAGE (with 400 mM imidazole-buffer), respectively, the appearance of a major peak of monomer and low intensity peaks of heteromeric species in MALDI-TOF-MS analysis is of a great advantage in determining the molecular mass accurately.

Insulin ($M_{MONO}$ 5729.6009; $M_{av}$ 5734.51) and apomyoglobin ($M_{MONO}$ 16940.9650; $M_{av}$ 16951.49) were used as internal standards for mass calibration while acquiring spectra. The $M_{av}$ of Hpn was determined as 6945.66±0.34 Da calculated from the average of at least five different measurements. A representative calibrated peak of Hpn[$M^+$] with *m/z* 6946.05 is shown in **Fig 3B**. However, MALDI-TOF-MS analysis confirmed that the $M_{av}$ of purified

recombinant Hpn was 6945.66±0.34 Da instead of the calculated molecular mass of 7,077 Da. This suggests the loss of the N-terminal methionine residue (*m/z* 149.21), probably in post-translation process in *E. coli* and this observation is consistent with the previous reports [4,5].

**Fig 3. Molecular mass analysis of Hpn with MALDI-TOF-MS.**

A. Sharp peak of monomeric Hpn together with neighboring small peak of matrix adduct, and three oligomeric species with lower intensity was observed in Hpn spectrum. The monomeric and three oligomeric species: $M^+$, $2M^+$, $3M^+$, and $4M^+$ with masses of *m/z* 6942.09, 13874.39, 20807.59, 27740.62 respectively are shown in inset.

B. Molecular mass of Hpn was measured (*m/z* 6946.05) using two different internal standards (insulin and apomyoglobin), which showed peaks for protonated and doubly charged species. Average MW of recombinant Hpn (without methionine) determined (6945.66±0.34) is showing almost negligible difference (0.35) compared to theoretical MW (6946.01).

## Hpn exhibits both “gel shifting” and “metal gel-shift”

The reduction by β-mercaptoethanol and boiling before gel loading of purified Hpn had no effect on the appearance of two bands even in different polyacrylamide-gel concentrations [(~14 kDa and ~18 kDa on 15% SDS-PAGE; **Fig 1C-E**) and (~7 kDa and <7 kDa on 20% SDS-PAGE; **Fig 4A**)]. This was further analyzed by $Ni^{2+}$ addition and removal (using EDTA) separately to the purified Hpn. In both cases, samples with and without boiling were analyzed in order to assess if Hpn showed a characteristic property of “heat modifiability” like outer membrane proteins (OMPs) from *E. coli* [51]. The concept of heat modifiability constitutes preservation of both folded and unfolded structures upon SDS treatment to purified OMPs but with no heat and shows two different bands on SDS-PAGE. Heating denatures the folded β-content of OMPs and SDS-PAGE data shows single band. No difference in migration pattern was observed between heated and non-heated samples of Hpn indicating the absence of heat modifiability (**Fig 4A**).

**Fig 4. Confirmation of "Metal gel-shift" mechanism.**

A. Effect of EDTA and $Ni^{2+}$ ion treatment on migration rate of recombinant Hpn in SDS-PAGE (polyacrylamide-gel 20%). Lane M, protein marker; lane 1 and 2, Hpn before and after boiling (3 min at 100ºC), respectively; lanes 3 and 4, EDTA-treated Hpn without and with boiling, respectively; lanes 5 and 6, $Ni^{2+}$-treated Hpn without and with boiling, respectively.

B. The SDS-PAGE analysis of partially-metalated-Hpn (25 μM) treated with increasing concentration of $Ni^{2+}$ (1:0, 1:0.8, 1:1.2, 1:1.6, 1:2.0, 1:2.4, 1:2.8, 1:3.2, 1:3.6, 1:4.0, 1:6.0 and 1:8.0). Equal volume of heat-denatured protein applied in each lane.

C. Scheme used for MALDI-TOF-MS analysis of Hpn protein that was heat denatured in Laemmli buffer. MS data was measured for Hpn treated with or without $Ni^{2+}$ ion (1:6 mol equivalent ratios). Further, MS data for Hpn (with or without $Ni^{2+}$) treated in Laemmli buffer (before and after SDS-PAGE) was measured. Even though some interference due to adducts was observed in samples treated with Laemmli buffer or gel-eluted fractions, metalated peaks (showing Hpn-$Ni^{2+}$ complexes) were distinct. The occurrence of metalated peaks was observed only for $Ni^{2+}$-treated Hpn in all the conditions.

Moreover, EDTA-treated Hpn showed only one band of ~7 kDa on 20% polyacrylamide-gel. On the other hand, the only protein band observed in $Ni^{2+}$-treated Hpn was of compact lower-size <7 kDa. Appearance of only one of the either band demonstrates that both bands were derived from same protein i.e. Hpn. The partially-metalated Hpn treated with relatively lower mol equivalent proportion of $Ni^{2+}$ (0.0, 0.8, 1.2, 1.6, 2.0, 2.4, 2.8, 3.2, 3.6, 4.0, 6.0 and 8.0) demonstrated gradual shift with decrease in homogeneity of upper band followed by increased intensity of compact lower band (**Fig4B**).

The Hpn protein treated for SDS-PAGE analyses was directly used for MALDI-TOF-MS measurements and mass spectra of $Ni^{2+}$-treated Hpn only showed peaks for protein-metal complexes (**Fig 4C**). The mass spectra of protein fractions eluted from SDS-gel corresponding to ~7 kDa and compact <7 kDa on 20% gel were measured. Only lower compact band (<7 kDa) confirmed mass spectra for partially preserved protein-metal complexes (**Fig 4C**). This MS data prompted us to quantify the metal-content of SDS-gel-

eluted bands. The $Ni^{2+}$ content in lower compact bands (combining several gel slices together) was detectable in ICP-OES. Measurements for EDTA-treated Hpn band were below the detection limit signifying no metal bound to Hpn protein.

Several studies have reported preservation of protein-metal complex in SDS-PAGE **(supporting information, S2 Table in S1 file)** and also in MALDI technique (**Table 3**). Thus, those studies have provided experimental evidence that some metal-binding proteins/metalloproteins can retain protein-metal complex even after using "harsh" experimental protocols (i.e. use of SDS, denaturing agents, acidic matrices, organic solvents or heating). Therefore, it is postulated that the methodology employed in the present study was able to detect Hpn-$Ni^{2+}$ complex and it was not a consequence of artifact formation. Previous circular dichroism (CD) studies have reported more compact structure (an increase in β-sheet with reduced α-helical content) after $Ni^{2+}$ binding to Hpn [5,6].

Taken together, these data indicate that preserved protein-metal complex forms a more compact structure leading to faster migration on SDS-PAGE. This phenomenon of reversible shift in position when treated with either EDTA or $Ni^{2+}$ was termed as "metal gel-shift".

## Polyacrylamide-gel concentration determines migration rate of Hpn on SDS-PAGE regardless of "metal gel-shift"

Polyacrylamide-gel concentration can dictate the migration speed of some polypeptides [31]. To test the hypothesis that "metal gel-shift" is related to only $Ni^{2+}$ binding to Hpn or whether gel percentage has an effect on it, we thoroughly analyzed gel mobility of apo-Hpn and $Ni^{2+}$-treated Hpn with different polyacrylamide-gel concentrations. This concept was investigated with purified Hpn after removing trace amounts of $Ni^{2+}$ (**Fig 5A**). The migration distance of apo-Hpn and $Ni^{2+}$-treated Hpn relative to marker proteins (Nacalai Tesque, Inc. Japan) was analyzed using ImageJ software [52] (**protocol provided in**

**Supporting information, Annexure A in S1 file**). Outcomes from these experiments were in agreement with our hypothesis; the $Ni^{2+}$-treated Hpn migrated faster than untreated Hpn showing MW difference of 3-4 kDa (**Fig 5B**). These results demonstrated that apo-Hpn migrated slowly in contrast to $Ni^{2+}$-treated Hpn in all analyzed polyacrylamide-gel concentrations, signifying that "metal gel-shift" is intimately associated with $Ni^{2+}$-binding to Hpn. This also shows that higher polyacrylamide-gel concentrations resulted in faster migration of both the forms on SDS-PAGE (with and without $Ni^{2+}$).

**Fig 5. Effect of polyacrylamide-gel concentration on migration speed of recombinant Hpn without or with metal-treatment on SDS-PAGE.**

A. Relative position of apo- and $Ni^{2+}$-treated Hpn protein depending on the polyacrylamide percentage (15, 18, 20 and 22.5%) in gels. The SDS-gel electrophoresis was done till bromophenol blue dye reached to the bottom in all gels. Therefore, theoretical MW values for marker proteins- lysozyme (14.4 kDa) and Trypsin inhibitor (21.5 kDa) were taken into consideration for estimation of apparent MW using ImageJ software (protocol provided in Supplementary information as Annexure A). Red dotted line depicts expected position corresponding to theoretical MW (~6.9 kDa).

B. The apparent MW of apo- and $Ni^{2+}$-treated Hpn separated on different polyacrylamide-gel concentrations was estimated by comparing relative migration distance of Hpn with globular marker proteins on SDS-PAGE.

## Analysis of non-covalent Hpn-$Ni^{2+}$ complexes

We evaluated inter-conversion of Hpn-metal complexes using purified Hpn by MALDI-TOF-MS. Although non-covalent complexes are expected to be stable at physiological pH, acidic conditions or organic solvents used in matrix preparation may not be the only factors important in the dissociation and prevent detection of these complexes in MALDI analysis [53]. In this work, we applied full-length Hpn protein for studying $Ni^{2+}$ binding. First, we standardized the set of conditions for acquisition of spectra for intact Hpn,

569 and then we investigated different types of matrices to analyze protein-metal ion complexes.
570 Among the tested combinations of acidic and non-acidic matrices, we found a mildly acidic
571 matrix (100% ACN, 0.01% TFA, and distilled water; v:v, 50:10:40) was most suitable in our
572 experimental conditions, and this was used in subsequent spectral measurements. This is the
573 first study reporting the successful application of MALDI-TOF-MS for investigating protein-
574 $Ni^{2+}$ ion complexes. The MS data showed the progressive appearance of all possible metal-
575 bound species of Hpn, signifying that binding of metal ions at each site on protein may occur
576 independently. Moreover, a decrease in spectral intensity of the apo-protein with increasing
577 amounts of $Ni^{2+}$ and increased intensity of metalated species provided conclusive evidence
578 for the binding of $Ni^{2+}$ to Hpn.

579 To evaluate $Ni^{2+}$ binding, Hpn treated with increasing molar concentrations of $NiSO_4$
580 solution was analyzed. Generally, the peaks of protein-metal complexes are smaller than the
581 peak of the apo-protein, even if a protein-metal interaction is already known to exist.
582 Therefore, higher amounts of $Ni^{2+}$ were added to Hpn after confirming that no obstruction
583 was caused by it in the MALDI spectrum. $Ni^{2+}$ solution was added to apo-Hpn (25 µM), pH
584 7.5 at an increasing mol equivalent ratio of Hpn to $Ni^{2+}$ ion. After 1 h incubation at room
585 temperature, protein-metal solution was mixed with matrix and MS were acquired as
586 described above (**Fig 6**).

587

588 **Fig 6. MALDI-TOF-MS analysis of $Ni^{2+}$ binding to Hpn.**
589 A. Spectra obtained with increasing concentrations of $Ni^{2+}$ (1:0, 1:1, 1:2.5, 1:5, 1:10, 1:20
590 and 1:40, mol equivalent from top to bottom, respectively) added to apo-Hpn (25 µM) shown
591 in the right panel, and enlarged view of three representative spectra (1:0, 1:10 and 1:40)
592 shown with molecular mass of each peak in the left side. Numbers above dotted line
593 correspond to the number of $Ni^{2+}$ bound to Hpn protein.
594 B. Mass difference calculated between adjacent peaks was found to be approximately equal
595 to the molecular mass of the $Ni^{2+}$ ion (58.69) with the loss of two $H^+$ atoms (molecular

596 weight [MW] of $H^+$ =1.00794) upon metal binding.

597 C. Model of $Ni^{2+}$ ion binding to Hpn. Order of occurrence has drawn on the basis of peak
598 intensity obtained in MALDI-TOF-MS data.

599

600 Representative MS of metalated species of Hpn clearly detected a progression with
601 seven major peaks (at *m/z* 6937.66, 6993.06, 7049.55, 7105.76, 7162.59, 7218.94, and
602 7275.33). The MS showed peaks of diverse intensity ranging from two to six $Ni^{2+}$ ions bound
603 to Hpn (**Fig 6A**), with no specific species dominant in all the measured protein to metal ratios.
604 The mass differences between adjacent peaks were about *m/z* 56.7 (**Fig 6B**), matching the
605 added $Ni^{2+}$ ion (*m/z* 58.69 of $Ni^{2+}$) with the loss of two hydrogen residues during the
606 ionization (*m/z* 1.007825×2). Overlay analysis of MS with and without $Ni^{2+}$ showed slight
607 mass differences (*m/z*) between expected and observed molecular masses may be due to
608 tightly bound ions as previously observed for UreE protein from *H. pylori* [54]. The seventh
609 and subsequent peaks were bifurcated possibly because of matrix adducts interference and
610 hence considered not reliable for assignment to Hpn-$Ni^{2+}$ ion complex. Titration of Hpn with
611 relatively lower $Ni^{2+}$ concentrations (1:5) indicated at least one preferential higher-affinity
612 site, peak intensities of the protein-metal complexes were not according to the loading
613 number of $Ni^{2+}$ ions on binding sites of Hpn (1>0>2>5>4>3). Furthermore, a difference in
614 peak intensity with higher amounts of $Ni^{2+}$ (1:40) was observed (3>4>2>5>6>1) suggesting
615 the presence of several binding sites with different affinity. The progressive appearance of
616 peaks for all of the possible Hpn-$Ni^{2+}$ ion complexes implied that $Ni^{2+}$ binding to Hpn
617 occurred in a non-cooperative way (**Fig 6C**) as reported in cysteine-rich human
618 metallothionein 1a [55] and histidine-rich *E. coli* SlyD protein [21].

## 619 $Ni^{2+}$ tolerance and accumulation in Hpn-expressing *E. coli* cells

620 If there is higher metal accumulation inside cells expressing the recombinant metal-
621 binding protein, then it should show better cell growth with higher tolerance compare with

wild-type upon addition of higher amounts of metal to the culture. However, this phenomenon was not observed in the current as well as previous studies in Hpn-producing *E. coli* cells (Hpn+) compared with wild-type (Hpn–) grown in LB medium [5]. Even though Hpn have more efficient metal-binding ability as observed in MALDI-TOF-MS analysis, higher $Ni^{2+}$ accumulation measured by ICP-OES (6× for Hpn+ compared with Hpn–) was not correlated with higher tolerance and cell survival (<twice in Hpn+ compared with Hpn–) (**Fig 7A-C**). We hypothesized that an unknown composition of nutrients in LB medium may compensate for toxicity or availability of free $Ni^{2+}$ ion to cells. Therefore, we tested M9 medium with a defined nutrient composition. As shown in **Fig 7D-E**, there was almost no further growth of wild-type (Hpn–) at 50 µM and 100 µM $Ni^{2+}$ supplied in M9 medium but Hpn producing cells (Hpn+) were grown normally with approximately 30 and 45 times higher intracellular $Ni^{2+}$ content respectively (**Fig 7F**).

**Fig 7. $Ni^{2+}$ tolerance, cell survival, and accumulation in Hpn-expressing *E. coli*.**
Effect of $Ni^{2+}$ on growth of *E. coli* in Luria-Bertani (LB) (panel A) and M9 medium (panel D). Growth curve was plotted in terms of optical density (OD) against amount of $Ni^{2+}$added to culture. Cell survival under $Ni^{2+}$ stress analyzed by dots blot as shown in panel B (LB) and E (M9). Panel C (LB) and F (M9) represent the intracellular $Ni^{2+}$ content in *E. coli* expressing *hpn* gene compare to that of without *hpn* gene.

# Discussion and Conclusions

The main findings of current work are as follows: 1) Hpn forms multimers in native state as well as SDS-resistant multimer when eluted with 400 mM imidazole in buffer; 2) $Ni^{2+}$-binding to Hpn altered antibody binding in western blot and ELISA signifying differential exposure of His-rich region upon metal-binding; 3) higher polyacrylamide-gel concentrations resulted in faster migration of Hpn in SDS-PAGE; 4) average molecular mass of Hpn determined as *m/z* 6945.66±0.34; 5) Hpn forms SDS-resistant (preserved) protein-metal complexes and exhibits metal-triggered shift in electrophoretic mobility causing "metal gel-shift" mechanism; 6) MALDI-TOF-MS was effectively employed to study non-covalent Hpn-$Ni^{2+}$ ion complexes showing up to six $Ni^{2+}$ ions bound per monomer in a non-cooperative way suggesting an equilibrium between Hpn-metalated species dependent on metal availability. These findings explore various unusual physicochemical aspects of Hpn. Also, higher tolerance and $Ni^{2+}$ accumulation in Hpn-expressing *Escherichia coli* than wild-type in minimal (M9) and nutrient-rich (LB) supply suggests protective role and potential to load higher amounts of $Ni^{2+}$ that corroborating with MALDI-TOF-MS data.

The Hpn protein contains remarkably high number of histidine residues, mostly in clusters (**Fig 1A**). Histidine is unique in its molecular structure with an imidazole ring in its side chain (an aromatic motif), and this can act as a ligand for metallic cations and as a hydrogen bond donor or acceptor. "Stacking" behavior of the aromatic rings of histidine can be one possible mechanism responsible for the formation of non-covalent multimeric complexes; however, this concept is yet to be understood clearly in multimeric proteins [56]. Elution buffer containing imidazole (400 μM) led to formation of SDS-resistant multimer that survived even in reduction and heat denaturation but converted to apparent monomer in denatured $Ni^{2+}$-treated Hpn (**Fig 5**). The preserved SDS-resistant protein-protein oligomer is

reported for several proteins under certain chemical environment (**Supporting information, S1 Table in S1 file**) [57–62].

## Gel shifting

Protein migration can be affected by several factors including molecular size, shape, net charge, MW of the protein, and polyacrylamide concentration [31]. SDS normally binds at hydrophobic sites, therefore it is reasonable that denatured apo-Hpn migrates at a slower rate compared with marker proteins, because of the higher amount of hydrophilic residues and only one hydrophobic amino acid in the Hpn [23,25,28]. A smaller protein with a higher number of hydrophilic residues may have a greater hydrodynamic radius than a larger protein but weaker hydration [63]. Similar results are reported for cystic fibrosis transmembrane conductance regulator for the reason that of a change in helical structure altered SDS-binding indicating protein-SDS complex size was a more important factor than net charge [23] and its interaction with the sieving effects of a polyacrylamide gel [25].

The SDS-PAGE data demonstrated that the polyacrylamide-gel concentration affects the migration rate of Hpn. Similar results are observed in “gel shifting” patterns for transmembrane proteins in SDS-PAGE [31]. This indicate as any factor that changes effective molecular size and net charge of protein-SDS complex can affect migration speed depending on polyacrylamide-gel concentration, specifically affecting its interaction with the available space in SDS-gel matrix [23,24,31]. In case of Hpn, impact of “stacking” behavior seems to exceed all other factors and may control the migration speed depending on polyacrylamide-gel concentration. Taken together, interplay between protein-protein interaction and sieving effects of gel matrix may be a significant factor that influences gel mobility.

## Metal gel-shift

Generally, non-covalent interactions should disrupt during SDS-PAGE owing to activity of SDS and reducing agent [60]. However, preservation of protein-metal complex in

SDS-PAGE is reported in several cases, possibly due to incomplete or "reconstructive denaturation" (**Supporting information, S2 Table in S1 file**) [35,36,60,62,64–69]. Preservation of partial Hpn-$Ni^{2+}$ complex even after electrophoretic separation implies significant strength and stability of Hpn-$Ni^{2+}$ bond. Although exact mechanism of resistance to reduction or denaturation and retaining metal ion is not yet known, similar results were observed in case of platinum-binding proteins [70].

The change in electrophoretic mobility on SDS-PAGE after metal-binding to a protein is rarely acknowledged except for some $Ca^{2+}$-binding proteins including calmodulin isoforms [36,37]. The wild-type and recombinant CDPKs from soybean [38], tobacco [39] and Arabidopsis [40] display shift in electrophoretic mobility on SDS-PAGE and migrate faster or slower depending on $Ca^{2+}$ availability and is probably due to $Ca^{2+}$-induced conformational change [40]. The protein band of apo-Hpn was not as sharp as that of $Ni^{2+}$-treated Hpn, which might be caused by conformational changes upon metal binding. Thus, higher degree of compactness or somehow altered SDS-binding to protein-metal complex that may allow faster migration of $Ni^{2+}$-treated Hpn than apo-Hpn. Faster migration on SDS-PAGE of unreduced against reduced lysozyme [71] and for a membrane protein OmpA [72] also suggested a possible role of structural compactness in "gel shifting". Considering added MW of metal ions, theoretical MW of Hpn protein in "metal-gel shift" band is higher than apo-Hpn band. On the contrary, "metal-gel shift" band is migrating faster to lower position compared to apo-Hpn band indicating conformational change (and not actual MW) is decisive in governing migration rate.

From the experimental results, mechanism of "gel shifting" and "metal gel-shift" can be described as shown in **Fig 8**. Anomalous migration of apo-Hpn (scheme highlighted with yellow background) or metal-bound Hpn (scheme highlighted with green background) might be due to differential amounts of SDS bound to protein, histidine stacking, altered

hydrodynamic radius, degree of compactness after metal-binding, or a combination of either of these factors. The different structures are illustrated and discussed thoroughly in **Fig 8**. Nevertheless, there might be additional biochemical and biophysical processes governing differential protein migration in SDS-PAGE that is not explained in this scheme.

**Fig 8. Probable interrelationship between differential electrophoretic mobility of Hpn and $Ni^{2+}$ binding.**

Hpn may not have a definite form in the absence of $Ni^{2+}$ (A). After denaturation (B), smaller amounts of SDS binding/stacking behavior/larger hydrodynamic radius as well as a combination of some or all of these conditions (C) might have resulted in slower migration on SDS-PAGE (scheme highlighted with yellow background). $Ni^{2+}$-treated Hpn forms a more compact structure (D). Pictorial structure of metalated Hpn is drawn to explain the model. MALDI spectra showed a partial $Ni^{2+}$ bound form (E) in denatured SDS-PAGE. Altered binding of SDS (F) caused by replacement of protein-protein to protein-SDS contacts (inhibiting stacking behavior) and/or degree of compactness (or reduced hydrodynamic radius) may be key factors responsible for "metal gel-shift" (scheme highlighted with green background). β-ME, β-mercaptoethanol; EDTA, ethylene diaminetetraacetic acid.

The binding of non-denatured Hpn to $Ni^{2+}$ column and reversible "metal-gel shift" in SDS-PAGE presented herein together with previous CD studies [5] indicated that Hpn protein could easily exchange metal ion suggesting the position of metal-binding domains are solvent exposed and present at Hpn surface. Metal-induced structural changes leading to the formation of a definite form has been reported for several other proteins, mostly associated with β-turns [21,73]. Accordingly, metal-binding region (not entirely hidden inside the structure of protein) could easily accessible for metal exchange and may involve small but unique structural rearrangements.

## Metal gel-shift and MS data

The pre-requisite for successful application of any mass spectrometry technique while

748 studying protein-metal interactions is the optimization of suitable method that preserves non-
749 covalent complexes. The MALDI technique has been used previously to study non-covalent
750 protein complexes (**Table 3**) by adjusting the range of parameters in order to preserve the
751 non-covalent interactions during acquisition of spectra [46,47,90].

752

753 **Table 3. List of non-covalent protein-metal ion interactions studied by MALDI in**
754 **combination with other methods.**

| Peptide | Metal | Matrix solution | Combined method | Reference |
|---|---|---|---|---|
| $(GHHPH)_5G$ peptide | Cu | DHB | TOF-MS | [74] |
| Human glycoprotein | Cu | DHB in 0.1% aqueous TFA | TOF-MS | [75] |
| Zinc finger peptides | Zn | HCCA in 1:l ammonium bicarbonate (1M)-ethanol. | - | [76] |
| Prion protein | Cu | DHB and 6,7-dihydroxycoumarin | TOF-MS | [77] |
| Ferrichrome | Fe | DHB in methanol | TOF-MS | [78] |
| Luteinizing hormone releasing hormone | Ni, Cu, Zn | Paranitroaniline in ethanol (10 mg/mL) | Fourier Transform-MS | [79] |
| Zinc finger peptide | Zn | 6-aza-2-thiothymine or DHB in Tris (10 mM), ammonium bicarbonate (20 mM) or 0.1% TFA | TOF-MS | [80] |
| Bradykinin | Cu, Ag, Co, Ni, Zn | HCCA matrix saturated in water and acetonitrile (70:30 v/v) containing 0.1% TFA. | TOF-MS | [81] |
| Prion proteins | Cu | Sinapinic acid in 20% acetonitrile | TOF-MS | [82] |
| Human brain proteins | Cu, Zn | DHB in acetonitrile and 0.1% TFA in water (2:1) | FT-ICR -MS | [83] |

| | | | | |
|---|---|---|---|---|
| Human tau proteins | Cu, Zn | DHB in acetonitrile and 0.1% TFA in water (2:1) | FT-ICR -MS | [84] |
| Human brain proteins | P, Cu, Zn, Fe | DHB in acetonitrile: 0.1% TFA in water (2:1) | FT-ICR-MS | [85] |
| Angiotensin I | Cu, K | HCCA, 3-aminoquinoline and glycerol | TOF-MS | [86] |
| Rat tissues | Zn, Cu, Fe, Cr, Cd, Pb | HCCA in acetonitrile:0.1% TFA in water (2:1) | TOF-MS and LA-ICP-MS | [87] |
| a-Crystallin | Zn | HCCA in 1:2 acetonitrile and 0.1 % TFA | TOF-MS | [88] |
| Protein fraction from Brazil nuts | Cu | HCCA in 50% acetonitrile and 0.1% TFA | TOF-MS | [89] |
| Hpn | Ni | Sinapinic acid (100% ACN, 0.01% TFA, and distilled water; v:v, 50:10:40) | TOF-MS | Present study |

(DHB: 2,5-dihydroxybenzoic acid; HCCA: α-cyano-4-hydroxycinnamic acid; FT-ICR-MS: Fourier transform-ion cyclotron resonance-mass spectrometry; LA-ICP-MS: Laser ablation-inductively coupled plasma-mass spectrometry)

Using mild-acidic matrix, spectral measurements showed distinct peaks, validating one apo-Hpn peak with six of Hpn-$Ni^{2+}$ complexes. Singly charged species of Hpn in MALDI-TOF-MS might allow detection of a sixth Hpn-$Ni^{2+}$ complex in mild-acidic conditions that not reported in previous studies [6,7]. However, appearance of weaker or non-specific protein-metal complexes due to higher amounts of metal added to protein samples is a limitation of the ionization process in positive mode measurements [21] and this possibility for sixth Hpn-$Ni^{2+}$ complex cannot be excluded. The interfaces of metal ions with histidine-rich peptides have not been investigated so far, perhaps because such peptides are not possible to study with routinely used techniques owing to overlapping signals [91]. Even though MS data alone are not sufficient to interpret the exact mechanism of metal-binding to various sites, these data have revealed the high flexibility (plasticity) of Hpn for $Ni^{2+}$ binding and its potential to load higher amounts of $Ni^{2+}$ in such a small structure of ~7 kDa.

Our MS data imply several key points that are complementary to “metal gel-shift”. At first, all available Hpn molecules were in metalated form at higher $Ni^{2+}$ in MS data. Similarly, presence of only “metal-gel shift” band at higher $Ni^{2+}$ was observed on SDS-PAGE (**Fig 4B**). Second, Hpn showed MS peaks for metalated species even treated with lower metal concentrations (**Fig 6**). This coincides with the appearance of "metal-gel shift" band in all protein-metal molar ratios (lower to higher) on SDS-PAGE (**Fig 4B and C**). Third, mass spectral intensity for apo-Hpn gradually decreased in $Ni^{2+}$-treated Hpn and subsequently mass spectral intensity for either of the metalated species was increased in respective measurements showing progressive appearance of Hpn-$Ni^{2+}$ peaks. This is also consistent with the gradual increase in heterogeneity of apo-Hpn band followed by compact "metal-gel shift" band.

Interestingly, at relatively higher amount of $Ni^{2+}$, distribution of mass for each Hpn-$Ni^{2+}$ complex was highly heterogeneous in MS data but on contrary, SDS-PAGE showed only one compact protein band. Electrophoretic separation of metalated species having smaller mass difference of each added $Ni^{2+}$ (0.055 kDa) cannot be distinguished on regular SDS-PAGE owing to limited resolution. Also, several factors can affect the migration of each metalated species of Hpn on SDS-PAGE including consequence of boiling, Laemmli buffer components, re-arrangement of protein-protein, protein-metal, and/or protein-SDS interactions. But this is not the case in MS measurements. Moreover, previous studies suggested involvement of almost all the four cysteine residues in $Ni^{2}$-binding [5,10–12]. Therefore, partial or complete reduction of disulfide bonds in two pairs of cysteine residues may release some but not all metal ions bound to Hpn during “constructive” denaturation. It may produce partially-metalated Hpn species in equilibrium (observed in MS of protein fractions before and after SDS-PAGE, **Fig 4C**) that migrated as homogenous “metal gel-shift” band on SDS-PAGE. In addition, differential ionization efficiency and ion suppression effect

796 in MS may interfere in mass-to-charge ratio [92]. The thermodynamic structures of the apo-
797 protein for metalation and the fully metalated protein for demetalation may not be the same
798 [21]. Thus, without further structural studies, it is intricate to compare precise mass
799 distribution of metalated species on SDS-PAGE and further studies are under investigation.
800 Nevertheless, "metal-gel shift" together with MALDI-TOF-MS data establishes that the
801 positional shift is directly associated with metal-binding to Hpn and it is reversible upon
802 metal removal.

803 In brief, our study reveals a novel mechanism of "metal gel-shift" responsible for
804 shifts in electrophoretic gel mobility of $Ni^{2+}$-treated Hpn on SDS-PAGE signifying metal-
805 induced conformational changes. This property can be used to explore interactions between
806 histidine-rich proteins and surfactant to investigate how metal-binding to a histidine-rich
807 protein changes its confirmation and hydrophobic or electrostatic interactions.

808

809

810

811

812

813

814

815

816

# Conflict of interest

The authors declare that they have no conflicts of interest with the contents of this article.

# Author contributions

HH and EHM conceived the idea for the project, supervised the study, provided essential reagents and edited the manuscript. RMS conducted most of the experiments, analyzed the results and wrote the manuscript. YI and JM conducted *H. pylori* culture experiments including genome DNA extraction and gene cloning. All authors edited the manuscript, reviewed the results and approved the final draft of this manuscript.

# Acknowledgement

The protocol and facility to perform ELISA was kindly provided by Dr. T. Tsuboi and Dr. E. Takashima (Division of Malaria Research, Proteo-Science Center, Ehime University, Matsuyama, Ehime, Japan).

# References


1. Cheng T, Xia W, Wang P, Huang F, Wang J, Sun H. Histidine-rich proteins in prokaryotes: metal homeostasis and environmental habitat-related occurrence. Metallomics. 2013; 5: 1423. doi:10.1039/c3mt00059a
2. Koonin EV, Wolf YI. Genomics of bacteria and archaea: the emerging dynamic view of the prokaryotic world. Nucleic Acids Res. 2008; 36: 6688–6719. doi:10.1093/nar/gkn668
3. de Reuse H, Vinella D, Cavazza C. Common themes and unique proteins for the uptake and trafficking of nickel, a metal essential for the virulence of Helicobacter pylori. Front Cell Infect Microbiol. 2013; 3: 1–6. doi:10.3389/fcimb.2013.00094
4. Gilbert JV, Ramakrishna J, Sunderman FW, Wright A, Plaut AG. Protein Hpn□: Cloning and characterization of a histidine-rich metal-binding polypeptide in Helicobacter pylori and Helicobacter mustelae. 1995; 63: 2682–2688.
5. Ge R, Watt RM, Sun X, Tanner J a, He Q-Y, Huang J-D, et al. Expression and characterization of a histidine-rich protein, Hpn: potential for Ni2+ storage in Helicobacter pylori. Biochem J. 2006; 393: 285–93. doi:10.1042/BJ20051160
6. Ge R, Zhang Y, Sun X, Watt RM, He Q-Y, Huang J-D, et al. Thermodynamic and kinetic aspects of metal binding to the histidine-rich protein, Hpn. J Am Chem Soc. 2006; 128: 11330–1. doi:10.1021/ja062589t
7. Wegner SV, Ertem E, Sunbul M, He C. Metal-binding properties of Hpn from Helicobacter pylori and implications for the therapeutic activity of bismuth. Chem Sci. 2011; 2: 451. doi:10.1039/c0sc00411a
8. Mobley HL, Garner RM, Chippendale GR, Gilbert JV, Kane AV, Plaut AG. Role of Hpn and NixA of Helicobacter pylori in susceptibility and resistance to bismuth and other metal ions. Helicobacter. 1999; 4: 162–169. PMID: 10469190

9. Seshadri S, Benoit SL, Maier RJ. Roles of His-rich Hpn and Hpn-like proteins in Helicobacter pylori nickel physiology. J Bacteriol. 2007; 189: 4120–6. doi:10.1128/JB.01245-06

10. Witkowska D, Politano R, Rowinska-Zyrek M, Guerrini R, Remelli M, Kozlowski H. The coordination of NiII and CuII ions to the polyhistidyl motif of Hpn protein: Is it as strong as we think? Chem - A Eur J. 2012; 18: 11088–11099. doi:10.1002/chem.201200780

11. Chiera NM, Rowinska-Zyrek M, Wieczorek R, Guerrini R, Witkowska D, Remelli M, et al. Unexpected impact of the number of glutamine residues on metal complex stability. Metallomics. 2013; 5: 214–21. doi:10.1039/c3mt20166j

12. Rowinska-Zyrek M, Witkowska D, Bielinska S, Kamysz W, Kozlowski H. The -Cys-Cys- motif in Helicobacter pylori's Hpn and HspA proteins is an essential anchoring site for metal ions. Dalton Trans. 2011; 40: 5604–10. doi:10.1039/c1dt10187k

13. Vinella D, Fischer F, Vorontsov E, Gallaud J, Malosse C, Michel V, et al. Evolution of Helicobacter: Acquisition by gastric species of two histidine-rich proteins essential for colonization. PLoS Pathog. 2015; 11: 1–32. doi:10.1371/journal.ppat.1005312

14. Zhou Q, Qi S, Sun X, Ge R. The interaction of a histidine-rich protein hpn with the membrane mimics: implications for pathologic roles of Hpn in Helicobacter pylori. Helicobacter. 2014; 19: 129–35. doi:10.1111/hel.12109

15. Zeng YB, Zhang DM, Li H, Sun H. Binding of Ni2+ to a histidine- and glutamine-rich protein, Hpn-like. J Biol Inorg Chem. 2008; 13: 1121–1131. doi:10.1007/s00775-008-0397-0

16. Brayman TG, Hausinger RP. Purification, characterization, and functional analysis of a truncated Klebsiella aerogenes UreE urease accessory protein lacking the histidine-rich carboxyl terminus. J Bacteriol. 1996; 178: 5410–6. PMCID: PMC178359

17. Chan K-H, Li T, Wong C-O, Wong K-B. Structural Basis for GTP-dependent dimerization of hydrogenase maturation factor HypB. PLoS One. 2012; 7: e30547. doi:10.1371/journal.pone.0030547

18. Fu C, Olson JW, Maier RJ. HypB protein of Bradyrhizobium japonicum is a metal-binding GTPase capable of binding 18 divalent nickel ions per dimer. Proc Natl Acad Sci U S A. 1995; 92: 2333–2337. doi:10.1073/pnas.92.6.2333

19. Rey L, Imperial J, Palacios JM, Ruiz-Argüeso T. Purification of Rhizobium leguminosarum HypB, a nickel-binding protein required for hydrogenase synthesis. J Bacteriol. 1994; 176: 6066–6073. PMID: 7928968

20. Hottenrott S, Schumann T, Plückthun a, Fischer G, Rahfeld JU. The Escherichia coli SlyD is a metal ion-regulated peptidyl-prolyl cis/trans-isomerase. J Biol Chem. 1997; 272: 15697–701. doi:10.1074/jbc.272.25.15697

21. Kaluarachchi H, Sutherland DE, Young A, Pickering IJ, Stillman MJ, Zamble DB. The Ni(II)-binding properties of the metallochaperone SlyD. J Am Chem Soc. 2009; 131: 18489–18500. doi:10.1021/ja9081765

22. Jeon WB, Cheng J, Ludden PW. Purification and characterization of membrane-associated CooC protein and its functional role in the insertion of nickel into carbon monoxide dehydrogenase from Rhodospirillum rubrum. J Biol Chem. 2001; 276: 38602–38609. doi:10.1074/jbc.

23. Rath A, Glibowicka M, Nadeau VG, Chen G, Deber CM. Detergent binding explains anomalous SDS-PAGE migration of membrane proteins. Proc Natl Acad Sci U S A. 2009; 106: 1760–1765. doi:10.1073/pnas.0813167106

24. Shi Y, Mowery R a., Ashley J, Hentz M, Ramirez AJ, Bilgicer B, et al. Abnormal SDS-PAGE migration of cytosolic proteins can identify domains and mechanisms that control surfactant binding. Protein Sci. 2012; 21: 1197–1209. doi:10.1002/pro.2107

25. Tulumello DV, Deber CM. Positions of polar amino acids alter interactions between transmembrane segments and detergents. Biochemistry. 2011; 50: 3928–3935. doi:10.1021/bi200238g

26. Karch CM, Borchelt DR. Aggregation modulating elements in mutant human superoxide dismutase 1. Arch Biochem Biophys. Elsevier Inc.; 2010;503: 175–82. doi:10.1016/j.abb.2010.07.027

27. Cun S, Li H, Ge R, Lin MCM, Sun H. A Histidine-rich and Cysteine-rich Metal-binding Domain at the C Terminus of Heat Shock Protein A from Helicobacter pylori: Implication for nickel homeostasis and bismuth susceptibility. J Biol Chem. 2008; 283: 15142–15151. doi:10.1074/jbc.M800591200

28. Panayotatos N, Radziejewska E, Acheson A, Pearsall D, Thadani A, Wong V. Exchange of a single amino acid interconverts the specific activity and gel mobility of human and rat ciliary neurotrophic factors. J Biol Chem. 1993;268: 19000–3. Pubmed: 8395524

29. Hayward LJ. Decreased metallation and activity in subsets of mutant superoxide dismutases associated with familial amyotrophic lateral sclerosis. J Biol Chem. 2002; 277: 15923–15931. doi:10.1074/jbc.M112087200

30. Saha S, Biswas KH, Kondapalli C, Isloor N, Visweswariah SS. The Linker Region in Receptor Guanylyl Cyclases Is a Key Regulatory Module: mutational analysis of guanylyl cyclase C. J Biol Chem. 2009; 284: 27135–27145. doi:10.1074/jbc.M109.020032

31. Rath A, Cunningham F, Deber CM. Acrylamide concentration determines the direction and magnitude of helical membrane protein gel shifts. Proc Natl Acad Sci U S A. 2013; 110: 15668–73. doi:10.1073/pnas.1311305110

32. Lee A, Rourke JO, Ungria MCDE, Robertson B, Daskalopoulos G, Dixon MF. A

941 standardized mouse model of Helicobacter pylori infection: introducing the Sydney
942 strain. 1997; 112: 1386–1397. PMID: 9098027
943 33. Raab A, Pioselli B, Munro C, Thomas-Oates J, Feldmann J. Evaluation of gel
944 electrophoresis conditions for the separation of metal-tagged proteins with subsequent
945 laser ablation ICP-MS detection. Electrophoresis. 2009; 30: 303–314.
946 doi:10.1002/elps.200800264
947 34. Sussulini A, Becker JS. Combination of PAGE and LA-ICP-MS as an analytical
948 workflow in metallomics: state of the art, new quantification strategies, advantages
949 and limitations. Metallomics. 2011;3: 1271. doi:10.1039/c1mt00116g
950 35. Otzen D. Protein-surfactant interactions: A tale of many states. Biochim Biophys Acta
951 - Proteins Proteomics; 2011; 1814: 562–591. doi:10.1016/j.bbapap.2011.03.003
952 36. Köhler C, Neuhaus G. Characterisation of calmodulin binding to cyclic nucleotide-
953 gated ion channels from Arabidopsis thaliana. FEBS Lett. 2000; 471: 133–136.
954 doi:10.1016/S0014-5793(00)01383-1
955 37. Damiani E, Margreth A. Subcellular fractionation to junctional sarcoplasmic
956 reticulum and biochemical characterization of 170 kDa Ca(2+)- and low-density-
957 lipoprotein-binding protein in rabbit skeletal muscle. Biochem J. 1991; 277: 825–832.
958 PMID: 1872815
959 38. Li J, Lee YJ, Assmann SM. Guard Cells Possess a Calcium-Dependent Protein Kinase
960 That Phosphorylates the KAT1 Potassium Channel 1. Plant Physiol. 1998; 116: 785–
961 795. PMID: 9489023
962 39. Yoon GM, Cho HS, Ha HJ, Liu JR, Lee HP. Characterization of NtCDPK1, a
963 calcium-dependent protein kinase gene in Nicotiana tabacum, and the activity of its
964 encoded protein. Plant Mol Biol. 1999; 39: 991–1001. PMID: 10344204
965 40. Romeis T, Franz S, Ehlert B, Liese A, Kurth J, Cazale A. Calcium-Dependent Protein

966 Kinase CPK21 Functions in Abiotic Stress Response in Arabidopsis thaliana. 2011; 4.
967 doi:10.1093/mp/ssq064
968 41. Akiyama H, Kanai S, Hirano M, Miyasaka H. A novel plasmid recombination
969 mechanism of the marine cyanobacterium Synechococcus sp. PCC7002. DNA Res.
970 1998; 5: 327–34. Pubmed: 10048481
971 42. Yamauchi S, Ueda Y, Matsumoto M, Inoue U, Hayashi H. Distinct features of protein
972 folding by the GroEL system from a psychrophilic bacterium, Colwellia
973 psychrerythraea 34H. Extremophiles. 2012; 16: 871–882. doi:10.1007/s00792-012-
974 0483-7
975 43. Laemmli UK. Cleavage of structural proteins during the assembly of the head of
976 bacteriophage T4. Nature; 1970. pp. 680–685. doi:10.1038/227680a0
977 44. Miura K, Orcutt AC, Muratova O V., Miller LH, Saul A, Long CA. Development and
978 characterization of a standardized ELISA including a reference serum on each plate to
979 detect antibodies induced by experimental malaria vaccines. Vaccine. 2008; 26: 193–
980 200. doi:10.1016/j.vaccine.2007.10.064
981 45. Jin Y, Manabe T. High-efficiency protein extraction from polyacrylamide gels for
982 molecular mass measurement by matrix-assisted laser desorption/ionization-time of
983 flight-mass spectrometry. Electrophoresis. 2005; 26: 1019–1028.
984 doi:10.1002/elps.200410187
985 46. Schlosser G, Pocsfalvi G, Malorni A, Puerta A, de Frutos M, Vekey K. Detection of
986 immune complexes by matrix-assisted laser desorption/ionization mass spectrometry.
987 Rapid Commun Mass Spectrom. 2003; 17: 2741–2747. doi:10.1002/rcm.1239
988 47. Rom S, Gilad A, Kalifa Y, Konrad Z, Karpasas MM, Goldgur Y, et al. Mapping the
989 DNA- and zinc-binding domains of ASR1 (abscisic acid stress ripening), an abiotic-
990 stress regulated plant specific protein. Biochimie. 2006; 88: 621–628.

991 doi:10.1016/j.biochi.2005.11.008

992 48. Mahadev SR, Hayashi H, Ikegami T, Abe S, Morita EH. Improved Protein
993 Overexpression and Purification Strategies for Structural Studies of Cyanobacterial
994 Metal-Responsive Transcription Factor, SmtB from Marine Synechococcus sp. PCC
995 7002. Protein J. 2013; 32: 626–634. doi:10.1007/s10930-013-9525-y

996 49. Watanabe Y, Aburatani K, Mizumura T, Sakai M, Muraoka S, Mamegosi S, et al.
997 Novel ELISA for the detection of raw and processed egg using extraction buffer
998 containing a surfactant and a reducing agent. J Immunol Methods. 2005; 300: 115–
999 123. doi:10.1016/j.jim.2005.02.014

1000 50. Lechtzier V, Hutoran M, Levy T, Kotler M, Brenner T, Steinitz M. Sodium dodecyl
1001 sulphate-treated proteins as ligands in ELISA. J Immunol Methods. 2002; 270: 19–26.
1002 doi:10.1016/S0022-1759(02)00214-4

1003 51. Burgess NK, Dao TP, Stanley AM, Fleming KG. -Barrel Proteins That Reside in the
1004 Escherichia coli Outer Membrane in Vivo Demonstrate Varied Folding Behavior in
1005 Vitro. J Biol Chem. 2008; 283: 26748–26758. doi:10.1074/jbc.M802754200

1006 52. Abràmoff MD, Magalhães PJ, Ram SJ. Image processing with imageJ. Biophotonics
1007 Int. 2004; 11: 36–41. doi:10.1117/1.3589100

1008 53. Strupat K. Molecular Weight Determination of Peptides and Proteins by ESI and
1009 MALDI. 2005; 405: 1–36. doi:10.1016/S0076-6879(05)05001-9

1010 54. Shi R, Munger C, Asinas A, Benoit SL, Miller E, Matte A, et al. Crystal Structures of
1011 Apo and Metal-Bound Forms of the UreE Protein from Helicobacter pylori : Role of
1012 Multiple Metal Binding Sites,. Biochemistry. 2010; 49: 7080–7088.
1013 doi:10.1021/bi100372h

1014 55. Sutherland DEK, Stillman MJ. Noncooperative cadmium(II) binding to human
1015 metallothionein 1a. Biochem Biophys Res Commun. 2008; 372: 840–844.

1016 doi:10.1016/j.bbrc.2008.05.142

1017 56. Liao S-M, Du Q-S, Meng J-Z, Pang Z-W, Huang R-B. The multiple roles of histidine
1018 in protein interactions. Chem Cent J. 2013; 7: 44. doi:10.1186/1752-153X-7-44

1019 57. Kolodziejski PJ, Rashid MB, Eissa NT. Intracellular formation of “undisruptable”
1020 dimers of inducible nitric oxide synthase. Proc Natl Acad Sci U S A. 2003; 100:
1021 14263–8. doi:10.1073/pnas.2435290100

1022 58. Atwood CS, Scarpa RC, Huang X, Moir RD, Jones WD, Fairlie DP, et al.
1023 Characterization of copper interactions with Alzheimer amyloid □?? peptides:
1024 Identification of an attomolar-affinity copper binding site on amyloid □β 1-42. J
1025 Neurochem. 2000; 75: 1219–1233. doi:10.1046/j.1471-4159.2000.0751219.x

1026 59. Tham SJ, Chang CD, Huang HJ, Lee YF, Huang TS, Chang CC. Biochemical
1027 characterization of an acid phosphatase from thermus thermophilus. Biosci Biotechnol
1028 Biochem. 2010;74: 727–735. doi:JST.JSTAGE/bbb/90773 [pii]

1029 60. Nowakowski AB, Wobig WJ, Petering DH. Native SDS-PAGE: high resolution
1030 electrophoretic separation of proteins with retention of native properties including
1031 bound metal ions. Metallomics. 2014;6: 1068–78. doi:10.1039/c4mt00033a

1032 61. Bullis BL, Li X, Rieder C V., Singh DN, Berthiaume LG, Fliegel L. Properties of the
1033 Na+/H+ exchanger protein detergent-resistant aggregation and membrane
1034 microdistribution. Eur J Biochem. 2002; 269: 4887–4895. doi:10.1046/j.1432-
1035 1033.2002.03202.x

1036 62. Pinato O, Musetti C, Farrell NP, Sissi C. Platinum-based drugs and proteins:
1037 Reactivity and relevance to DNA adduct formation. J Inorg Biochem. 2013;122: 27–
1038 37. doi:10.1016/j.jinorgbio.2013.01.007

1039 63. Erickson HP. Size and shape of protein molecules at the nanometer level determined
1040 by sedimentation, gel filtration, and electron microscopy. Biol Proced Online. 2009;

11: 32–51. doi:10.1007/s12575-009-9008-x

64. Solis C, Oliver A, Andrade E. PIXE analysis of proteins from a photochemical center. Nucl. Instr. Meth. Phys. Res. Sect. B, 1998; 136: 928–931. Available: http://www.sciencedirect.com/science/article/pii/S0168583X97008963

65. Binet MRB, Ma R, McLeod CW, Poole RK. Detection and characterization of zinc- and cadmium-binding proteins in Escherichia coli by gel electrophoresis and laser ablation-inductively coupled plasma-mass spectrometry. Anal Biochem. 2003; 318: 30–38. doi:10.1016/S0003-2697(03)00190-8

66. Gao Y, Chen C, Zhang P, Chai Z, He W, Huang Y. Detection of metalloproteins in human liver cytosol by synchrotron radiation X-ray fluorescence after sodium dodecyl sulphate polyacrylamide gel electrophoresis. Anal Chim Acta. 2003; 485: 131–137. doi:10.1016/S0003-2670(03)00347-7

67. Verbi FM, Arruda SCC, Rodriguez APM, Perez CA, Arruda MAZ. Metal-binding proteins scanning and determination by combining gel electrophoresis, synchrotron radiation X-ray fluorescence and atomic spectrometry. J Biochem Biophys Methods. 2005; 62: 97–109. doi:10.1016/j.jbbm.2004.09.008

68. Finney L, Chishti Y, Khare T, Giometti C, Levina A, Lay PA, et al. Imaging metals in proteins by combining electrophoresis with rapid X-ray fluorescence mapping. ACS Chem Biol. 2010; 5: 577–587. doi:10.1021/cb1000263

69. Weseloh G, Kuhbacher M, Bertelsmann H, Ozaslan M, Kyriakopoulos A, Knochel A, et al. Analysis of metal-containing proteins by gel electrophoresis and synchrotron radiation X-ray fluorescence. J Radioanal Nucl Chem. 2004; 259: 473–477. doi:10.1023/B:JRNC.0000020921.66046.1c

70. Mena ML, Moreno-Gordaliza E, Moraleja I, Canas B, Gomez-Gomez MM. OFFGEL isoelectric focusing and polyacrylamide gel electrophoresis separation of platinum-

1066 binding proteins. J Chromatogr A. 2011; 1218: 1281–1290.
1067 doi:10.1016/j.chroma.2010.12.115
1068 71. Pitt-Rivers R, Impiombato FS. The binding of sodium dodecyl sulphate to various
1069 proteins. Biochem J. 1968; 109: 825–830. PMCID: PMC1187034
1070 72. Kleinschmidt JH, Wiener MC, Tamm LK. Outer membrane protein A of E. coli folds
1071 into detergent micelles, but not in the presence of monomeric detergent. Protein Sci.
1072 1999; 8: 2065–2071. doi:10.1110/ps.8.10.2065
1073 73. Chen SH, Chen L, Russell DH. Metal-induced conformational changes of human
1074 metallothionein-2A: A combined theoretical and experimental study of metal-free and
1075 partially metalated intermediates. J Am Chem Soc. 2014; 136: 9499–9508.
1076 doi:10.1021/ja5047878
1077 74. Hutchens TW, Nelson RW, Yip T. Evaluation of Peptide / Metal Ion Interactions by
1078 UV Laser Desorption Time-of-flight Mass Spectrometry. J. Mol. Recogn. 1991; 4:
1079 151–153. doi: 10.1002/jmr.300040407
1080 75. Nelson RW, Hutchens TW. Mass spectrometric analysis of a transition-metal-binding
1081 peptide using mass spectrometry. A demonstration of probe tip chemistry. Rapid
1082 Commun Mass Spectrom 1992; 6: 4–8. doi: 10.1002/rcm.1290060103
1083 76. Woods AS, Buchsbaum JC, Worrall TA, Berg JM, Cotter RJ. Matrix-Assisted Laser
1084 Desorption/Ionization of Noncovalently Bound Compounds. Anal Chem. 1995; 67:
1085 4462–4465. doi:10.1021/ac00120a005
1086 77. Hornshaw MP, McDermott JR, Candy JM. Copper binding to the N-terminal tandem
1087 repeat regions of mammalian and avian prion protein. Biochem Biophys Res
1088 Commun. 1995; 207: 621–629. doi:10.1006/bbrc.1995.1233
1089 78. Kaltashov IA, Cotter RJ, Harry W, Ketner GW. Ferrichrome: Surprising stability of a
1090 cyclic peptide-FeIII complex revealed by mass spectrometry. J Am Soc Mass

Spectrom 1997; 8: 1070–1077. doi:10.1016/S1044-0305(97)00128-1

79. Masselon C, Salih B, Zenobi R. Matrix-assisted laser desorption/ionization Fourier transform mass spectrometry of luteinizing hormone releasing hormone-metal ion complexes. J Am Soc Mass Spectrom. 1999; 10: 19–26. doi:10.1016/S1044-0305(98)00128-7

80. Lehmann R, Zenobi R, Vetter S. Matrix-assisted laser desorption/ionization mass spectra reflect solution-phase zinc finger peptide complexation. J Am Soc Mass Spectrom. 1999; 10: 27–34. doi:10.1016/S1044-0305(98)00116-0

81. Cerda BA, Cornett L, Wesdemiotis C. Probing the interaction of alkali and transition metal ions with bradykinin and its des-arginine derivatives via matrix-assisted laser desorption/ionization and postsource decay mass spectrometry. Int J Mass Spectrom. 1999; 193: 205–226. doi: 10.1016/S1387-3806(99)00164-5

82. Qin K, Yang Y, Mastrangelo P, Westaway D. Mapping Cu(II) Binding Sites in Prion Proteins by Diethyl Pyrocarbonate Modification and Matrix-assisted Laser Desorption Ionization-Time of Flight (MALDI-TOF) Mass Spectrometric Footprinting. J Biol Chem. 2002; 277: 1981–1990. doi:10.1074/jbc.M108744200

83. Becker JS, Zoriy M, Becker JS, Pickhardt C, Damoc E, Juhacz G, et al. Determination of phosphorus-, copper-, and zinc-containing human brain proteins by LA-ICPMS and MALDI-FTICR-MS. Anal Chem. 2005; 77: 5851–5860. doi:10.1021/ac0506579

84. Becker JS, Zoriy M, Przybylski M, Becker JS. Study of formation of Cu- and Zn-containing tau protein using isotopically-enriched tracers by LA-ICP-MS and MALDI-FTICR-MS. J Anal At Spectrom. 2007; 22: 63–68. doi:10.1039/B609419H

85. Becker JS, Zoriy M, Przybylski M, Becker JS. High resolution mass spectrometric brain proteomics by MALDI-FTICR-MS combined with determination of P, S, Cu, Zn and Fe by LA-ICP-MS. Int J Mass Spectrom. 2007; 261: 68–73.

1116 doi:10.1016/j.ijms.2006.07.016

1117 86. Hortal AR, Hurtado P, Martínez-Haya B. Matrix-assisted laser desorption mass
1118 spectrometry of gas-phase peptide–metal complexes. Appl Phys A. 2008; 93: 935–939.
1119 doi:10.1007/s00339-008-4739-0

1120 87. Becker JS, Mounicou S, Zoriy M V., Becker JS, Lobinski R. Analysis of metal-
1121 binding proteins separated by non-denaturating gel electrophoresis using matrix-
1122 assisted laser desorption/ionization mass spectrometry (MALDI-MS) and laser
1123 ablation inductively coupled plasma mass spectrometry (LA-ICP-MS). Talanta. 2008;
1124 76: 1183–1188. doi:10.1016/j.talanta.2008.05.023

1125 88. Karmakar S, Das KP. Identification of histidine residues involved in Zn2+ binding to
1126 αA- and αB-Crystallin by chemical modification and MALDI TOF mass spectrometry.
1127 Protein J. 2012; 31: 623–640. doi:10.1007/s10930-012-9439-0

1128 89. Jayasinghe SB, Caruso JA. Preliminary investigation of Cu-containing proteins in
1129 seeds of Brazil nuts by ICPMS and MALDI-MS methods. Int J Mass Spectrom. 2013;
1130 356: 33–36. doi:10.1016/j.ijms.2013.09.014

1131 90. Chen F, Gülbakan B, Weidmann S, Fagerer SR, Ibáñez AJ, Zenobi R. Applying mass
1132 spectrometry to study non-covalent biomolecule complexes. Mass Spectrom Rev.
1133 2007; 26: 223–257. doi:10.1002/mas

1134 91. Witkowska D, Politano R, Rowinska-Zyrek M, Guerrini R, Remelli M, Kozlowski H.
1135 The coordination of NiII and Cu(II) ions to the polyhistidyl motif of Hpn protein: is it
1136 as strong as we think? Chemistry. 2012; 18: 11088–99. doi:10.1002/chem.201200780

1137 92. Szájli E, Fehér T, Medzihradszky KF. Investigating the quantitative nature of
1138 MALDI-TOF MS. Mol Cell Proteomics. 2008; 7: 2410–2418.
1139 doi:10.1074/mcp.m800108-mcp200

1140

# S1 Supporting Information

**Table S1. Proteins showing apparent SDS-resistant oligomeric forms upon denaturing SDS-PAGE.**

**Table S2. List of proteins retaining metal ion on SDS-PAGE.**

**Fig S1. Schematic diagrams of gene constructs and protein analysis by SDS-PAGE used for western blot and ELISA analysis.**

A. Schematic diagram of gene construct consisted of *gfp* fused with artificial His.tag (left panel) and GFP-His6 protein expression confirmed by SDS-PAGE (right panel).

B. Schematic diagram of *gfp* fused with *hpn* at C-terminal followed by stop codon (left panel) and recombinant protein of GFP-Hpn fusion analyzed by SDS-PAGE (right panel).

**Fig S2. Comparison of DNA sequence of *hpn* from *Helicobacter pylori* strain SS1 (this study) with strain 26695 (NCBI data).**

The promoter region and *hpn* gene of strain SS1 was PCR amplified and nucleotide sequence was compared with NCBI data of strain 26695 (GenBank accession number U26361). Putative promoter elements are shown in a box. The *hpn* gene region is shown in uppercase letters and mutations at the nucleotide level are shaded in gray. The putative terminator region of transcription is underlined. The promoter region was highly conserved in strain SS1 including Shine-Dalgarno sequence (GGAG) and promoter elements (-10 and -35).

**Fig S3. Separation of purified Hpn on non-denaturing blue native-PAGE.**

High molecular weight marker (GE Healthcare), abbreviated as HMW, was used in all gels [Thyroglobulin (669 kDa), Ferritin (440 kDa), Catalase (232 kDa), Lactate dehydrogenase:

(140 kDa) and Albumin (66 kDa)]. Recombinant Hpn (200 µM) was treated with either 1 mM of EDTA or $Ni^{2+}$ independently and then applied to 10% native-gel. Apparent multimeric complexes of >670, ~500, ~230 kDa were observed in presence or absence of $Ni^{2+}$ and EDTA.

**Annexure S1.**

Protocol followed for analysis of apparent MW of Hpn on SDS-PAGE in Fig. 5.

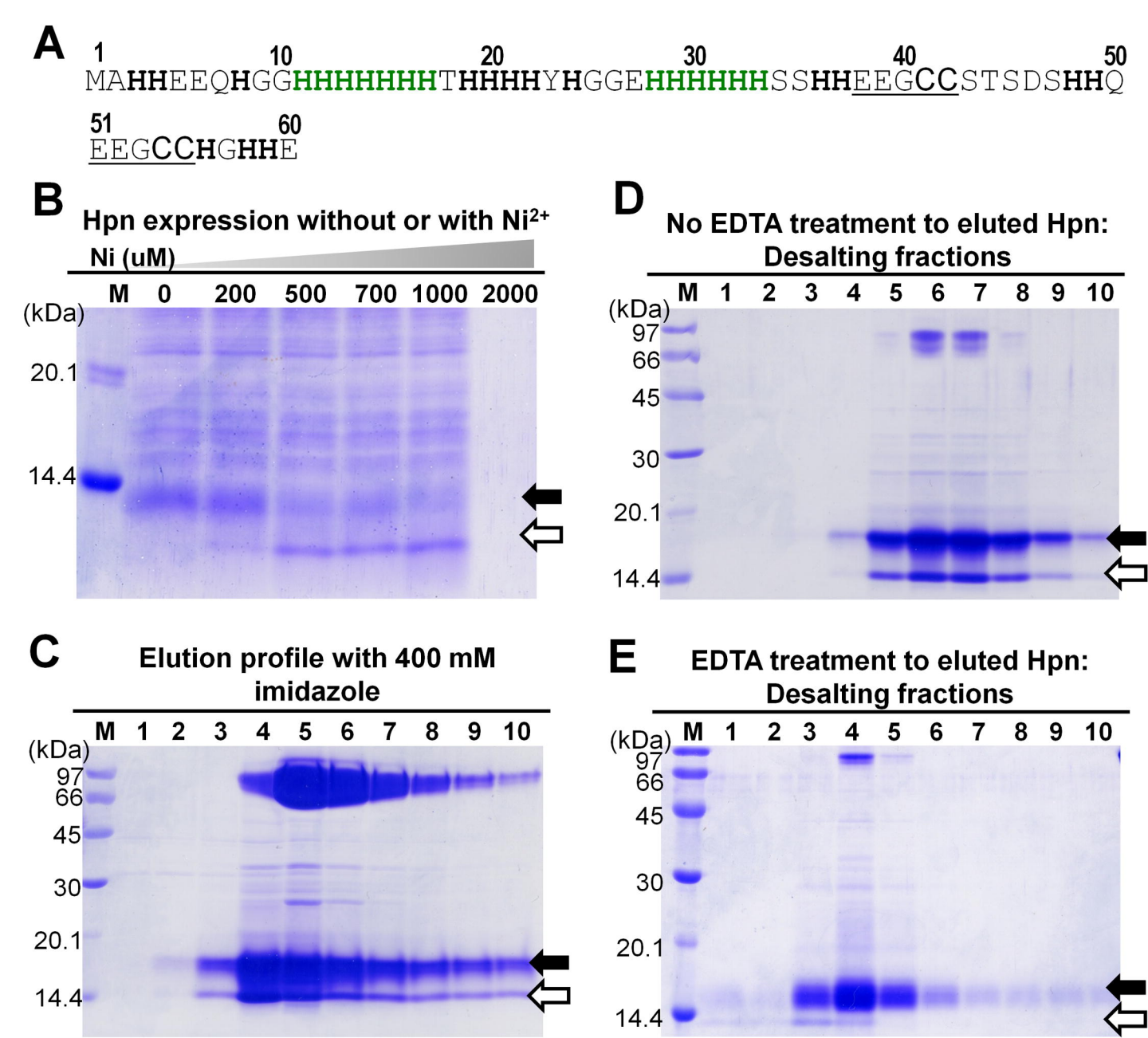
A
1 10 20 30 40 50
MAHHEEQHGGHHHHHHHTHHHHYHGGEHHHHHHSSHHEEGCCSTSDSHHQ
51 60
EEGCCHGHHE
B
Hpn expression without or with Ni2+
Ni (uM)
M 0 200 500 700 1000 2000
(kDa)
20.1
14.4
D
No EDTA treatment to eluted Hpn: Desalting fractions
M 1 2 3 4 5 6 7 8 9 10
(kDa)
97
66
45
30
20.1
14.4
C
Elution profile with 400 mM imidazole
M 1 2 3 4 5 6 7 8 9 10
(kDa)
97
66
45
30
20.1
14.4
E
EDTA treatment to eluted Hpn: Desalting fractions
M 1 2 3 4 5 6 7 8 9 10
(kDa)
97
66
45
30
20.1
14.4

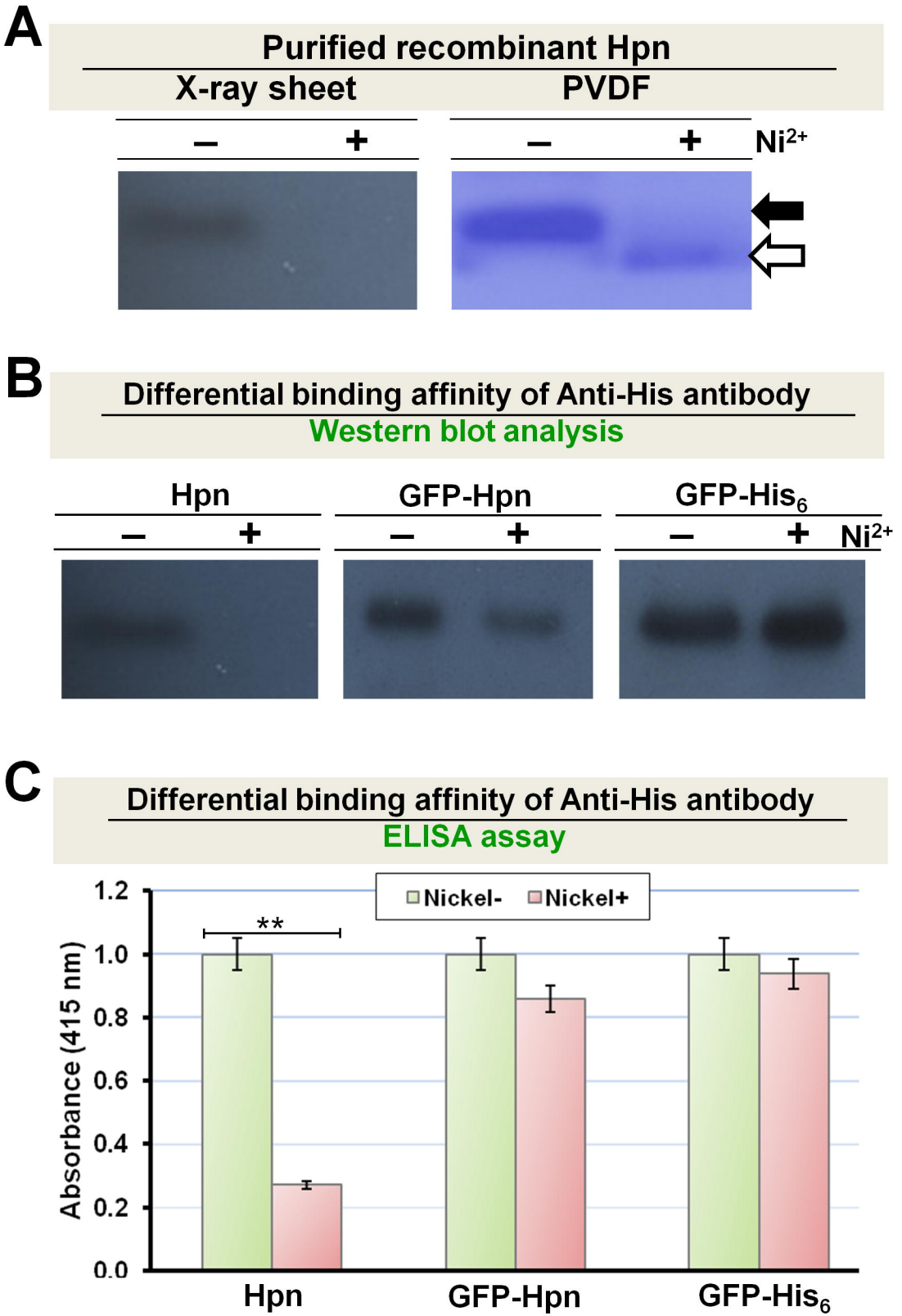
A
Purified recombinant Hpn
X-ray sheet
PVDF
–
+
–
+
Ni2+
B
Differential binding affinity of Anti-His antibody
Western blot analysis
Hpn
GFP-Hpn
GFP-His6
–
+
–
+
–
+
Ni2+
C
Differential binding affinity of Anti-His antibody
ELISA assay
Nickel-
Nickel+
**
Absorbance (415 nm)
1.2
1.0
0.8
0.6
0.4
0.2
0.0
Hpn
GFP-Hpn
GFP-His6

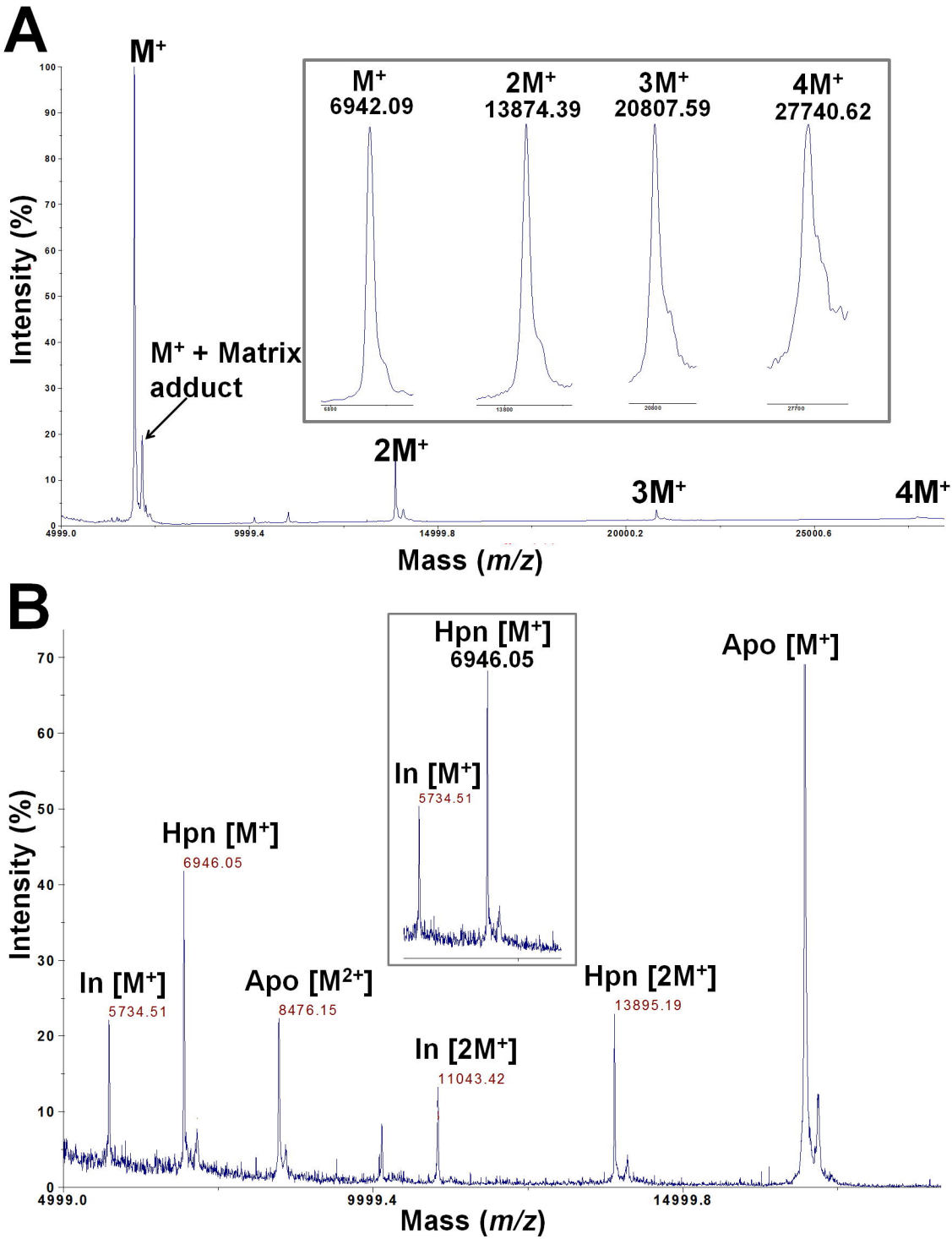
A
M+
M+ + Matrix adduct
2M+
3M+
4M+
M+ 6942.09
2M+ 13874.39
3M+ 20807.59
4M+ 27740.62
Intensity (%)
Mass (m/z)
B
Hpn [M+] 6946.05
In [M+] 5734.51
Apo [M+]
Hpn [M+] 6946.05
In [M+] 5734.51
Apo [M2+] 8476.15
In [2M+] 11043.42
Hpn [2M+] 13895.19
Intensity (%)
Mass (m/z)

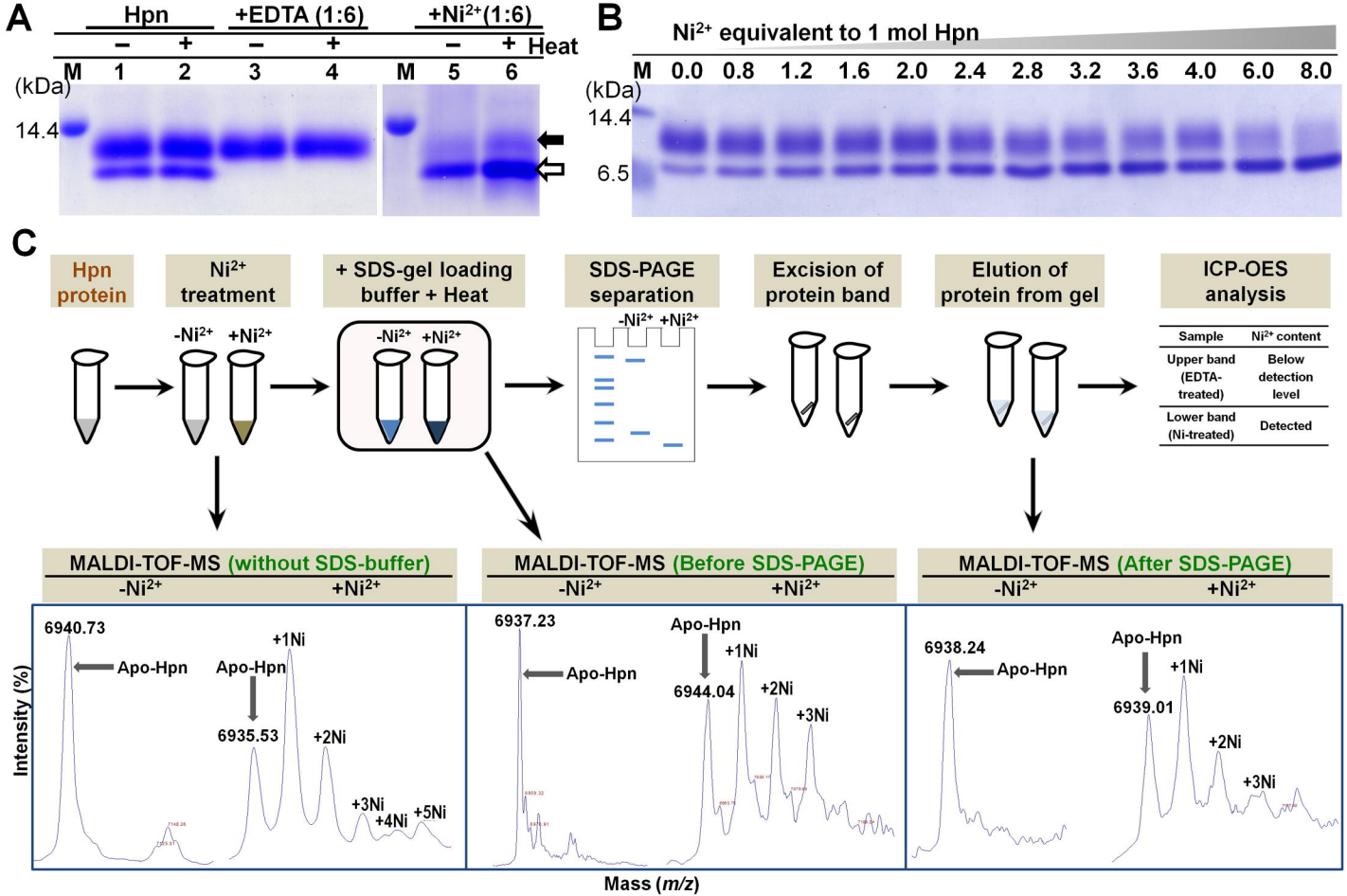
A
Hpn
+EDTA (1:6)
+Ni2+(1:6)
– + – + – + Heat
M 1 2 3 4 M 5 6
(kDa)
14.4
B
Ni2+ equivalent to 1 mol Hpn
M 0.0 0.8 1.2 1.6 2.0 2.4 2.8 3.2 3.6 4.0 6.0 8.0
(kDa)
14.4
6.5
C
Hpn protein
Ni2+ treatment
+ SDS-gel loading buffer + Heat
SDS-PAGE separation
Excision of protein band
Elution of protein from gel
ICP-OES analysis
-Ni2+ +Ni2+
Sample | Ni2+ content
Upper band (EDTA-treated) | Below detection level
Lower band (Ni-treated) | Detected
MALDI-TOF-MS (without SDS-buffer)
MALDI-TOF-MS (Before SDS-PAGE)
MALDI-TOF-MS (After SDS-PAGE)
-Ni2+ +Ni2+
6940.73
Apo-Hpn
6935.53
+1Ni
+2Ni
+3Ni
+4Ni
+5Ni
6937.23
6944.04
6938.24
6939.01
Intensity (%)
Mass (m/z)

**A**

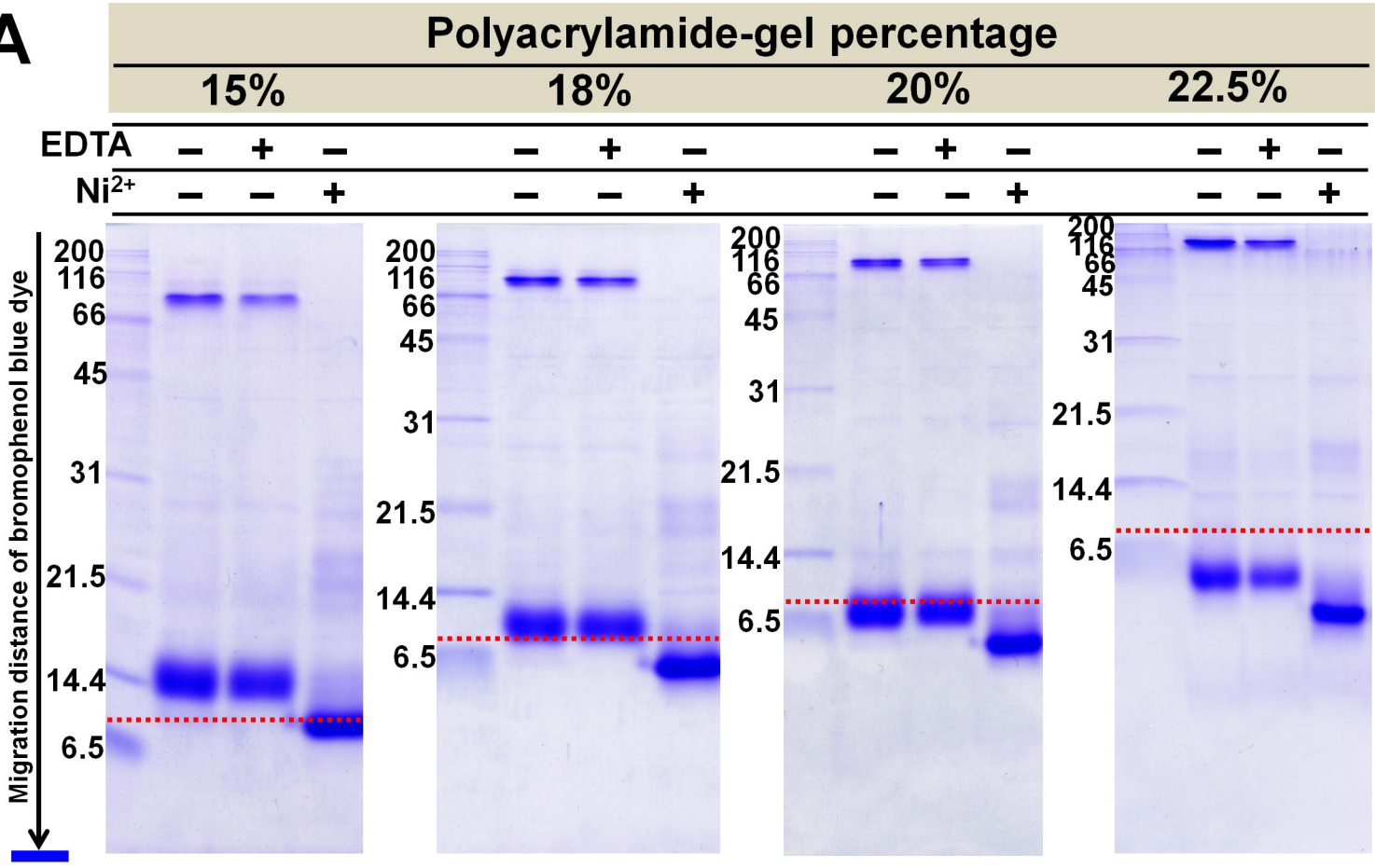


**B**

| Polyacrylamide-gel | 15 % | 18 % | 20 % | 22.5 % |
|---|---|---|---|---|
| Apo-Hpn (kDa) | 14.7 | 11.7 | 9.7 | 4.9 |
| $Ni^{2+}$-Hpn (kDa) | 11.3 | 8.2 | 6.4 | 0.8 |
| Difference between Apo-Hpn and $Ni^{2+}$-Hpn (kDa) | 3.4 | 3.5 | 3.3 | 4.1 |

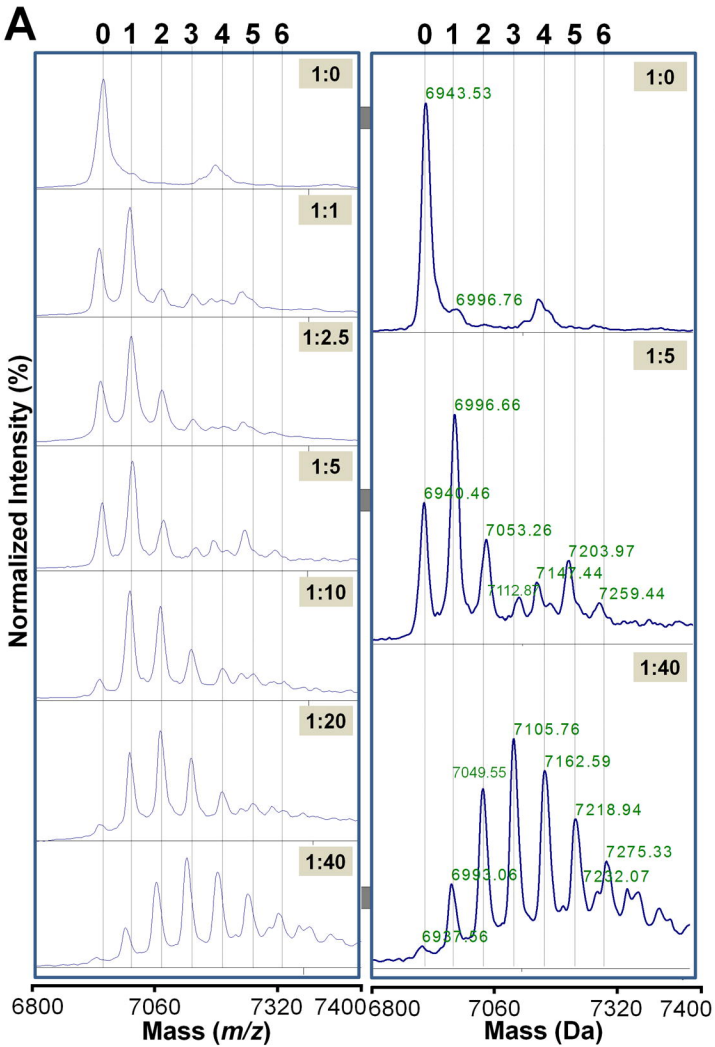


B

**Mass difference between adjacent peaks**

| Label | 0 | 1 | 2 | 3 | 4 | 5 | 6 |
|---|---|---|---|---|---|---|---|
| MW | 6937.6 | 6993.0 | 7049.5 | 7105.7 | 7162.5 | 7218.9 | 7275.3 |
| Difference | - | 55.4 | 56.49 | 56.21 | 56.83 | 56.35 | 56.39 |

C

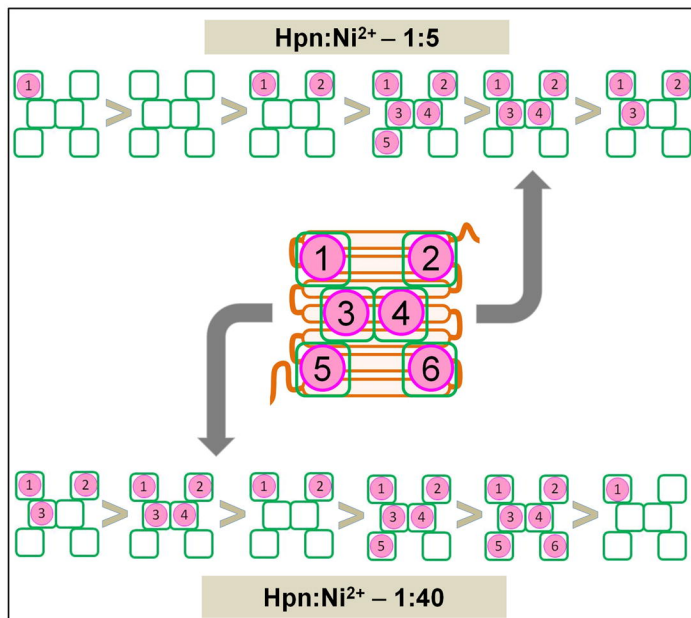

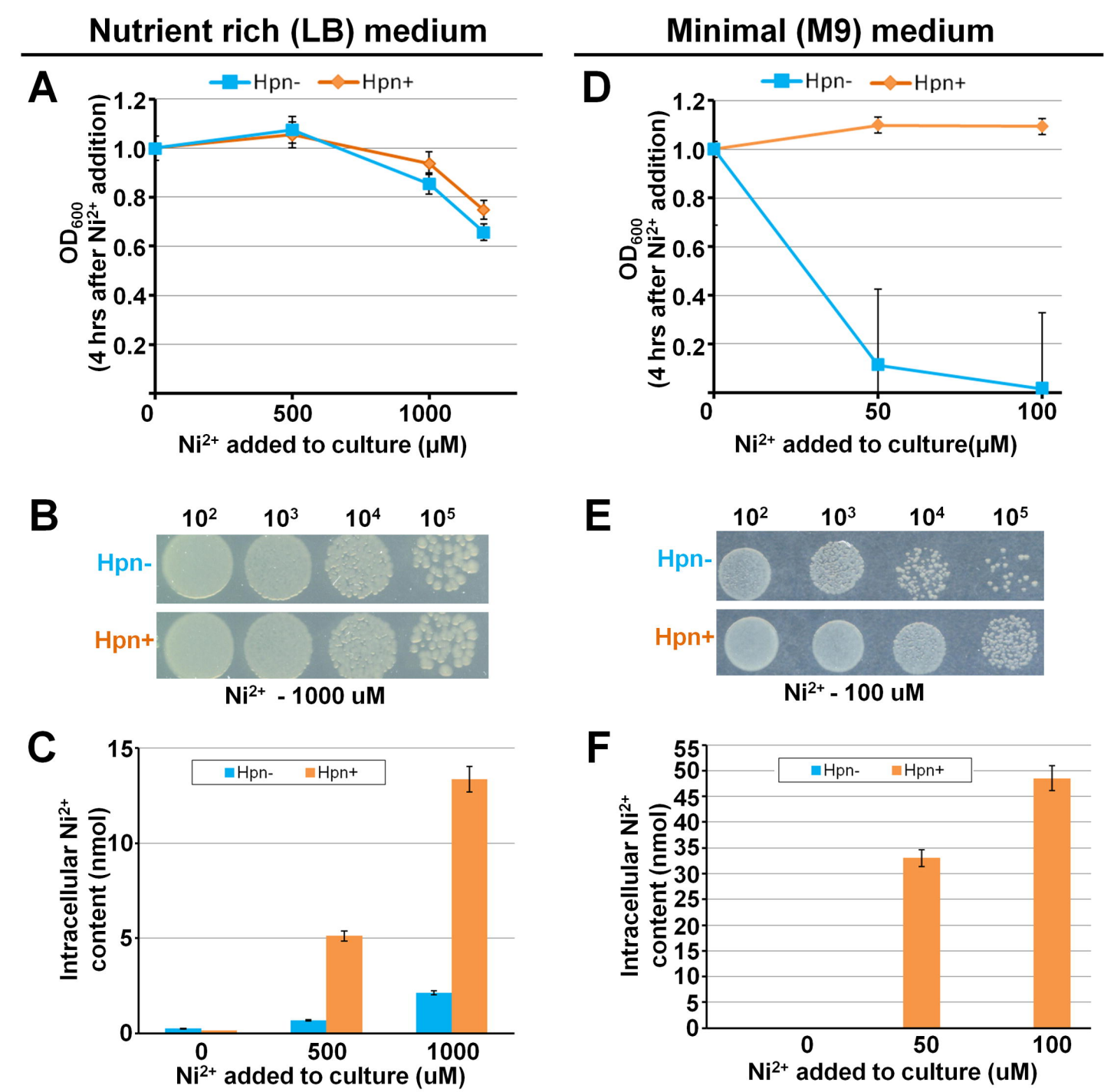
Nutrient rich (LB) medium
Minimal (M9) medium
A
Hpn-
Hpn+
OD600 (4 hrs after Ni2+ addition)
1.2
1.0
0.8
0.6
0.4
0.2
0
500
1000
Ni2+ added to culture (μM)
D
Hpn-
Hpn+
OD600 (4 hrs after Ni2+ addition)
1.2
1.0
0.8
0.6
0.4
0.2
0
50
100
Ni2+ added to culture(μM)
B
10^2
10^3
10^4
10^5
Hpn-
Hpn+
Ni2+ - 1000 uM
E
10^2
10^3
10^4
10^5
Hpn-
Hpn+
Ni2+ - 100 uM
C
Hpn-
Hpn+
Intracellular Ni2+ content (nmol)
15
10
5
0
0
500
1000
Ni2+ added to culture (uM)
F
Hpn-
Hpn+
Intracellular Ni2+ content (nmol)
55
50
45
40
35
30
25
20
15
10
5
0
0
50
100
Ni2+ added to culture (uM)

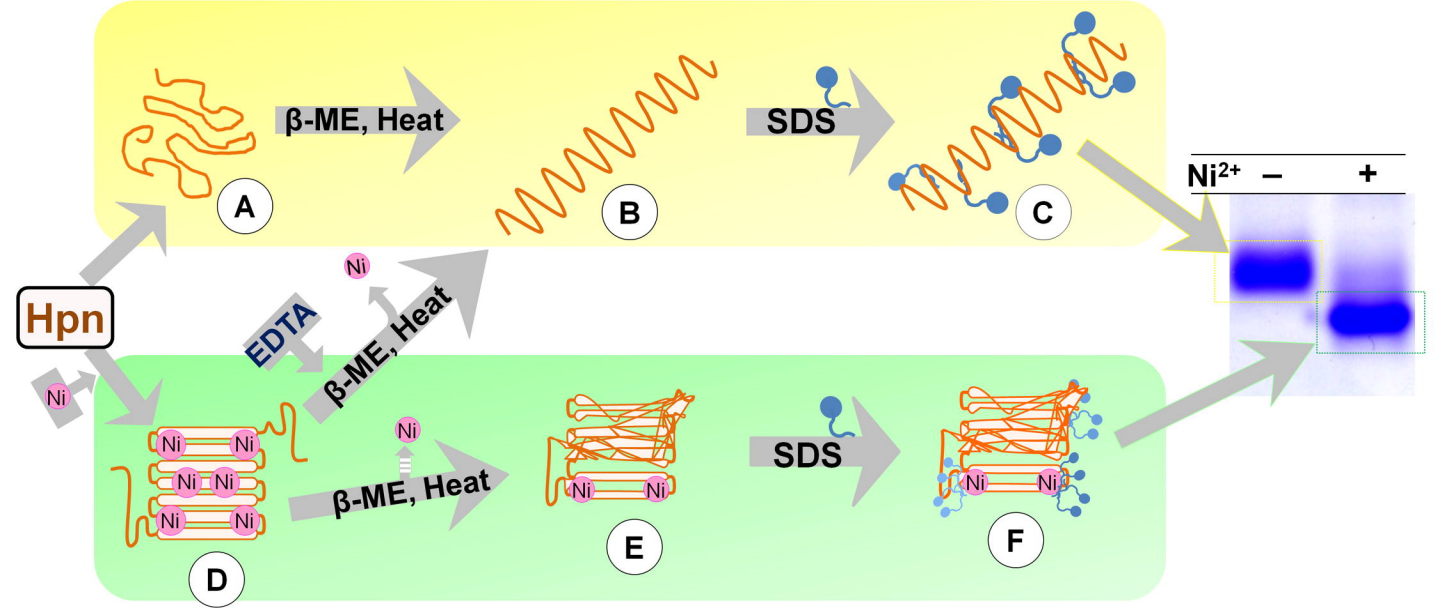
β-ME, Heat
SDS
A
B
C
Ni2+ – +
Hpn
Ni
EDTA
Ni
β-ME, Heat
Ni
Ni
Ni
Ni
Ni
Ni
β-ME, Heat
Ni
Ni
Ni
SDS
Ni
Ni
D
E
F